

Accurate tracking of locomotory kinematics in mice moving freely in three-dimensional environments

Marker-based MoCap in Mice

Authors:

Bogna M. Ignatowska-Jankowska, Lakshmi Priya I. Swaminathan, Tara H. Turkki,
Dmitriy Sakharuk, Aysen Gurkan Ozer, Alexander Kuck, Marylka Yoe Uusisaari

Author Contributions:

- **BIJ:** Designed research, Performed research, Analyzed data, Wrote the paper.
- **LIS:** Performed research.
- **THT:** Performed research.
- **DS:** Analyzed data.
- **AGO:** Performed research.
- **AK:** Performed research.
- **MYU:** Designed research, Performed research, Analyzed data, Wrote the paper.

Correspondence: Marylka Yoe Uusisaari (uusisaari@oist.jp)

Manuscript details:

- Number of Figures: 8 + 5 supplementary
- Number of Tables: 0
- Number of Multimedia: 13 videos
- Abstract: 243 words
- Significance Statement: 111 words

- Introduction: 706 words
- Discussion: 1899 words

Acknowledgements:

The authors are grateful for the help and support provided by the Animal Resources Section (ARS) of Core Facilities at Okinawa Institute of Science and Technology Graduate University, as well as the entire Neuronal Rhythms in Movement (nRIM) unit at OIST for helpful discussions.

Data availability: Trajectory data in non-processed form will be made available at [data repository name].

Code availability: All code for result generation will be made available at [GitHub repository address].

Conflict of Interest: Authors report no conflict of interest.

Funding sources:

This research was supported by OIST intramural funds, as well as a Japan Society for Promotion of Science (JSPS) Fellowship for Overseas Researchers (P17388), Kakenhi Grant-in-Aid for JSPS Fellows (17F17388), and Kakenhi Grant for Scientific Research (21K06399) awarded to Bogna M. Ignatowska-Jankowska. Tara H. Turkki is supported by a fellowship from Osk. Huttunen Foundation.

1 Accurate tracking of locomotory kinematics in
2 mice moving freely in three-dimensional
3 environments

4 **Abstract**

5 Marker-based motion capture (MBMC) is a powerful tool for precise, high-
6 speed, three-dimensional tracking of animal movements, enabling detailed study
7 of behaviors ranging from subtle limb trajectories to broad spatial exploration.
8 Despite its proven utility in larger animals, MBMC has remained underutilized
9 in mice due to the difficulty of robust marker attachment during unrestricted
10 behavior. In response to this challenge, markerless tracking methods, facilitated
11 by machine learning, have become the standard in small animal studies due to
12 their simpler experimental setup. However, trajectories obtained with markerless
13 approaches at best approximate ground-truth kinematics, with accuracy strongly
14 dependent on video resolution, training dataset quality, and computational
15 resources for data processing.

16 Here, we overcome the primary limitation of MBMC in mice by implanting min-
17 imally invasive markers that remain securely attached over weeks of recordings.
18 This technique produces high-resolution, artifact-free trajectories, eliminating the
19 need for extensive post-processing. We demonstrate the advantages of MBMC
20 by resolving subtle drug-induced kinematic changes that become apparent
21 only within specific behavioral contexts, necessitating precise three-dimensional
22 tracking beyond simple flat-surface locomotion. Furthermore, MBMC uniquely

23 captures the detailed spatiotemporal dynamics of harmaline-induced tremors,
24 revealing previously inaccessible correlations between body parts and thus
25 significantly improving the translational value of preclinical tremor models.
26 While markerless tracking remains optimal for many behavioral neuroscience
27 studies in which general posture estimation suffices, MBMC removes barriers to
28 investigations demanding greater precision, reliability, and low-noise trajectories.
29 This capability significantly broadens the scope for inquiry into the neuroscience
30 of movement and related fields.

31 1 Significance statement

32 Studying fine-scale motor behaviors in mice demands data with precision and fidelity
33 that markerless approaches often struggle to provide. While marker-based motion cap-
34 ture is the gold standard for high-resolution kinematic analysis, its use in freely moving
35 mice has been limited by challenges in marker use. This work overcomes these barriers
36 by introducing implantable markers with replaceable reflective heads, fundamentally
37 transforming the feasibility of robust high-definition 3D tracking across a wide range
38 of behaviors and experimental conditions. By enabling the detection of subtle phe-
39 nomena, such as harmaline-induced tremors, with spatiotemporal detail unmatched
40 by markerless tracking, this approach provides a powerful tool for advancing studies
41 of motor control and sensorimotor integration in rodents.

42 2 Introduction

43 Currently, high-precision kinematic tracking in rodents necessary for probing
44 (dys)function of movement-related neural circuits is largely based on restricting ani-
45 mal movement [1] or creating artificial environments (such as transparent floors or
46 locomotion in narrow confines) that can distort behavior and limit the translational

47 potential of results. As the emerging translational crisis has highlighted weaknesses in
48 animal experimental designs [2–5], their improvement is needed to reflect more accu-
49 rately the complexity of behavior. For example, it is rare for wild mice to explore flat
50 and smooth surfaces, which are often used in experimental behavioral settings. Instead,
51 the natural behavior of most rodents involves locomoting in uneven terrain with com-
52 plex demands for body kinematics: they balance, climb, jump, and swim. Assessment
53 of such 3D kinematics in freely behaving rodents requires the use of high-precision 3D
54 motion capture.

55 The superior resolving power of marker-based motion capture (MBMC) in general,
56 as compared to markerless systems, stems from the massive improvement in signal-
57 to-noise ratio (by filtering out components unrelated to tracked points) as well as
58 the on-camera compression of high-resolution image data to compact 2D coordinates.
59 These aspects eliminate many of the signal processing bottlenecks necessary for mark-
60 erless tracking. Furthermore, dedicated infrared illumination of retroreflective markers
61 eliminates noise related to changing ambient lighting conditions.

62 Despite its precision, robustness, and common use in humans and other large ani-
63 mals [6–10], use of marker-based 3D motion capture in small animals such as mice and
64 rats has been limited by technical difficulties [1, 5, 8, 11–14] and markerless animal
65 tracking has become the main tool for assessing behavior ([15]; see, e.g., DeepLabCut
66 [16–18], SLEAP [19], DANNCE ([20]), MoSeq ([21, 22]), LightningPose [23]). These
67 approaches have recently experienced significant advances in flexibility and ease of use,
68 but achieving precise 3D trajectory tracking remains a challenge [5, 22, 24–26]. Even
69 in human studies, markerless techniques usually show only limited agreement with
70 marker-based methods even under optimal conditions and typically generate mean
71 errors of 10% [7–10, 12, 13, 25–32]. Although dedicated markerless systems based on
72 deep learning can reach accuracy comparable to marker-based systems [33], their per-
73 formance depends on training data and variation between subject morphology (e.g.

⁷⁴ during aging), experimental conditions (e.g. subtle changes in lightning) and task char-
⁷⁵ acteristics (such as mode of locomotion) can lead to discrepancies. Importantly, the
⁷⁶ development of markerless technique accuracy is ultimately dependent on the com-
⁷⁷ parison with ground truth data, for which x-ray imaging [34] or MBMC data are
⁷⁸ needed.

⁷⁹ In order to obtain precise kinematic recordings in mice that move freely in a
⁸⁰ three dimensional environment, we took advantage of a marker-based 3D motion cap-
⁸¹ ture system (Qualisys, Gothenburg, Sweden; [35–37]) conventionally used to track
⁸² movement in humans and other large animals. Using a novel approach for perma-
⁸³ nent retroreflective skin-marker implantation as well as omitting enclosures between
⁸⁴ cameras and subjects that lead to unwanted reflections and spurious tracking errors,
⁸⁵ we obtain robust low-noise kinematic trajectories during various locomotory tasks
⁸⁶ without cumbersome machine learning-based post-processing commonly used to clean
⁸⁷ markerless or noisy marker-based trajectories [38]. Although the process of MBMC
⁸⁸ recording is somewhat more laborious than conventional behavioral video recording
⁸⁹ — requiring careful initial habituation of animals, consistent handling routines, and
⁹⁰ familiarization of experimenters with working freely moving animals in the absence of
⁹¹ enclosures — the quality of data and its ease of use (e.g., due to small raw file size)
⁹² are transformative for the straightforward application of analytical approaches.

⁹³ In this paper, we first quantify the tracking performance of MBMC in terms of
⁹⁴ continuity (gaps), accuracy, and noise ("jitter") using mice fitted with skin-implanted,
⁹⁵ retroreflective markers during exploration of a relatively conventional open field
⁹⁶ recording arena. Next, we demonstrate how the MBMC approach facilitates examina-
⁹⁷ tion of mouse movements across various spatio-temporal scales, such as simultaneous
⁹⁸ assessment of general locomotion and fast limb movements. Our findings reveal pre-
⁹⁹ viously unrecognized variations in mouse limb dynamics during different locomotor
¹⁰⁰ scenarios. We also show that even well-known drug effects (such as those observed

101 after cannabinoid receptor activation; [39]) can be surprisingly different when examined
102 in horizontal vs. vertical locomotion, underscoring the importance of employing a
103 broader spectrum of behavioral settings. Finally, to showcase the resolution of MBMC,
104 we track harmaline-induced tremor and show a significant correlation of motion across
105 the whole animal body.

106 **3 Methods**

107 **3.1 Experimental subjects and drug administration**

108 Adult male C57BL/6A mice (CLEA, Japan), aged 10–12 weeks (20-25g) at the
109 beginning of the experiments, were used. Mice (n=29) were subjected to systemic
110 intraperitoneal drug administration followed by behavioral assessments. The ani-
111 mals were randomly assigned to drug treatments and tested in a counterbalanced
112 Latin square within-subject design, with at least a 72-hour washout period between
113 treatments.

114 Drug treatments were selected to induce locomotor disturbances through different
115 mechanisms of action. The CB1 and CB2 receptor agonist CP55,940 (Tocris, UK),
116 known to inhibit locomotor activity at doses of 1 mg/kg, was administered at a low
117 dose of 0.3 mg/kg to test whether subtle changes in fine kinematics could be observed
118 and to evaluate the sensitivity of the motion capture system. Harmaline, known to
119 induce rhythmic activity in the inferior olive and produce whole-body tremor, was
120 administered at a high dose of 20 mg/kg to examine the tremor-tracking potential of
121 MBMC. Doses were selected based on preliminary experiments and existing literature
122 ([40–42]).

123 The drugs were dissolved in a vehicle solution consisting of ethanol, Kolliphor, and
124 saline (1:1:18 ratio) and administered at volumes of 10 μ l/g for CP55,940 and 20 μ l/g
125 for harmaline. All drugs were administered 30 minutes before recordings. Investigators
126 were blinded to experimental conditions whenever possible.

¹²⁷ The animals were housed in a temperature (20–22°C) and humidity (55±10%)
¹²⁸ controlled, AAALAC-approved facility, with a 12/12-hour reversed light/dark cycle
¹²⁹ (lights on at 0700h and off at 1900h). They were kept in enriched environments with
¹³⁰ *ad libitum* access to food and water. All experiments were conducted during the
¹³¹ dark (active) phase of the circadian cycle. This study is reported in accordance with
¹³² ARRIVE guidelines ([43]).

¹³³ 3.2 Marker implantation procedure

¹³⁴ Marker implantation was performed 11–14 days before the start of behavioral exper-
¹³⁵ iments to ensure full healing. We used male C57BL/6A mice (CLEA Japan), aged
¹³⁶ 10–12 weeks and weighing 20–25 g at the time of implantation. Distances for marker
¹³⁷ placement should be adjusted when working with larger or smaller animals.

¹³⁸ Markers were placed across the shoulder blades, lumbar spine, hips, and along the
¹³⁹ tibia between the knees and ankles. These locations were selected to enable tracking of
¹⁴⁰ whole-body movement during locomotion, postural adjustments, and finer kinematic
¹⁴¹ features such as tremor, miscoordination, or swaying.

¹⁴² The total weight of all uncoated markers (1260–1270 mg) remained within 5–7%
¹⁴³ of the animals' body weight. The implants caused no visible discomfort, remained
¹⁴⁴ stable for over a year, and enabled repeated within-subject testing. Their subcutaneous
¹⁴⁵ anchoring to connective tissue ensured more faithful tracking of skeletal movement
¹⁴⁶ than skin-surface markers, which are susceptible to slippage on the loose rodent skin.

¹⁴⁷ Under isoflurane anesthesia (2–3%, Somnosuite, Kent Scientific, CT, USA), the fur
¹⁴⁸ around planned implant sites was shaved. Mice were positioned symmetrically on the
¹⁴⁹ surgical platform with hind legs bent such that the feet formed a line perpendicular
¹⁵⁰ to the body's long axis. The skin was cleaned with 70% ethanol, and anatomical
¹⁵¹ landmarks were marked—specifically, the midline between the hips and between the
¹⁵² shoulder blades.

153 A total of five pairs of stainless steel markers were implanted subcutaneously at
154 designated body locations (Figure 1). Each implant consisted of a short steel rod (<14
155 mm in length, 0.9–1.27 mm diameter; 18–20 gauge), capped with 3–4 mm diameter
156 screw-on stainless steel spheres. We used 6 mm piercings for the shoulder and lumbar
157 implants, 7 mm for the hips, and 8 mm for the legs.

158 A calibrated stick (e.g., a Q-tip marked using precise calipers) was used to mark
159 the placement of the paired holes. To ensure implant stability and reduce rejection,
160 the skin bridge between holes was made to be at least twice the length of the piercing
161 shaft. For example, for hip markers spaced 14 mm apart, symmetrical dots were drawn
162 centered on the midpoint of the hips. For lumbar spine placement, a dot was marked
163 8–10 mm above the hip center, and paired lumbar holes were placed 14 mm apart.

164 For the upper leg markers, the knee position was marked with the leg in both
165 maximally bent and half-bent positions. The hole was placed between these two knee
166 positions to accommodate joint movement. The lower leg marker was positioned 14 mm
167 above the heel, centered on the calf. The total distance from heel to upper leg marker
168 was approximately 28 mm. Symmetry of all markings was verified before piercing.

169 Careful placement of the lower leg holes is essential: holes placed too laterally may
170 allow the marker to slide behind the leg, making it invisible to cameras. The lower-leg
171 marker must be centered on the calf, and the ankle marker positioned high enough to
172 avoid ground contact when the mouse stands, preventing interference with walking.

173 At each marked location, a small (<1.5 mm) skin puncture was made using an
174 18G sterile needle. Each hole was then widened with super-fine forceps (e.g., Dumont
175 #55), and the disinfected steel rod part of the piercing (soaked in 70% ethanol for at
176 least 20 min) was inserted. The piercing was then secured with a screw-on ball on the
177 opposite end.

178 All implants were cleaned with ethanol and dried before insertion. During implan-
179 tation, the skin was gently lifted using forceps to minimize trauma. An excess fold

¹⁸⁰ of skin was left between the balls of each piercing, which naturally adjusted during
¹⁸¹ healing.

¹⁸² Mice were allowed to recover for 11–14 days before recording sessions began. During
¹⁸³ this period, behavioral training was initiated, but implant exchange or manipulation
¹⁸⁴ was avoided to ensure proper healing.

¹⁸⁵ **3.3 Behavioral training**

¹⁸⁶ To ensure accurate 3D tracking, no transparent surfaces or obstructions (e.g., trans-
¹⁸⁷ parent walls) can be present between the cameras and the experimental subject,
¹⁸⁸ as spurious reflections and distortions catastrophically degrade tracking performance
¹⁸⁹ (Figure 1a, b). Consequently, animals must be habituated to the naturally anxiogenic
¹⁹⁰ open field arena and so they will remain within the designated area during testing with-
¹⁹¹ out restriction of movement. We developed a dedicated protocol for animal training
¹⁹² to achieve these goals.

¹⁹³ **3.3.1 Handling and pre-training**

¹⁹⁴ Experiments began 11 to 14 days after marker implantation to allow proper wound
¹⁹⁵ healing and stable marker positioning. During this period, mice undergo handling,
¹⁹⁶ habituation, and task-training in the following sequence:

- ¹⁹⁷ 1. Handling sessions, lasting 2–3 days, familiarized mice with human interaction and
¹⁹⁸ included several steps. The animals were first taken out of their cages using a tube
¹⁹⁹ and then gently pulled by the base of the tail to the outer part of the experimenter’s
²⁰⁰ hand or forearm. This progressed to scooping the mice while holding their tails
²⁰¹ gently and finally to scooping without tail support.
- ²⁰² 2. Habitat in the arena for 5 to 7 days: Initially, mice were placed in a circular 30 cm
²⁰³ arena with 4 cm walls in a brightly lit room for 2 to 3 days. In the next phase lasting
²⁰⁴ 3–4 days, mice were placed in a circular arena without walls. If they attempted

205 to leave the arena, they were guided back by gently pulling their tails or, if only
206 partially leaving, by tapping their noses. The training lasted 2 to 5 minutes per
207 session. The training arena was distinct from the experimental arena to prevent
208 overhabituation and ensure robust exploratory behavior during experiments.

209 3. Task training followed habituation and included two components: vertical climbing
210 on a wheel (CLB) and running on a treadmill (TRM).

211 Each animal was subjected to the level of training that resulted in a similar perfor-
212 mance, and all animals are trained until they correctly perform the task as expected.
213 Positive or negative reinforcements were not used to facilitate training.

214 **3.3.2 Marker exchange process**

215 During the training period, the mice were also accustomed to the 3- to 5-minute
216 process of manual marker exchange to avoid the need for anesthesia. Outside recording
217 periods, the mice wore uncoated 3 mm steel screw-on spheres. These were exchanged
218 for larger retroreflective markers 15 minutes before recording and replaced with the
219 original spheres after the session.

220 **3.3.3 Behavioral experiment apparatuses**

221 Behavioral assessments were conducted within a $30 \times 30 \times 30$ cm volume surrounded
222 by cameras. The experimental apparatuses were placed within this volume. For OF
223 task, a 30×30 cm textured polyethylene surface was used as the "arena". For the CLB
224 task, the outer surface of a spoked running wheel (25 cm in diameter) designed for
225 rats was used. The wheel was manually moved to match voluntary mouse movements
226 (see Movie 3, [6.3](#)), and retroreflective markers were placed on its outer rim to track
227 movement. TRM running tasks were conducted on a motorized single-lane treadmill
228 (MazeEngineers, Boston, MA), with markers attached to the belt at 20 cm intervals
229 to monitor speed (see Movie 5, [6.5](#)). All apparatuses were cleaned between trials.

²³⁰ **3.4 Retroreflective marker fabrication**

²³¹ To achieve high retroreflectivity and durability suitable for rodent experiments, 4 mm
²³² stainless steel barbell piercing screw-on balls (Figure 1d) (Felio Co., Ltd., Tsukuba,
²³³ Japan) were used as the base. These markers were coated with three layers: (1) retrore-
²³⁴ flective tape (3M, MN, USA), (2) Linear Low Density Polyethylene (LLDPE) film
²³⁵ (TRUSCO Micron 25 X W X/300 m, TSF2550, Trustco, Japan), and (3) UV-curable
²³⁶ plastic (BD-SKCJ, Bondic, NY, USA).

²³⁷ Retroreflective tape was cut into narrow strips (6 mm width) and shaped into
²³⁸ slightly curved crescents approximately 1 mm wide. The strips were applied to the
²³⁹ marker with the edges slightly overlapping, covering the surface from back to front in
²⁴⁰ the coronal plane. A round area of uncovered metal on top of the sphere, approximately
²⁴¹ 1–2 mm in diameter, was further covered with a circular piece of reflective tape (2–4
²⁴² mm in diameter) to ensure uniform reflectivity.

²⁴³ To protect the fragile retroreflective tape from damage, a UV-curable plastic layer
²⁴⁴ was used as the outermost coating. However, direct contact with liquids or media other
²⁴⁵ than air distorts the reflectivity of the tape, rendering it ineffective. To preserve a layer
²⁴⁶ of air between the plastic and the retroreflective tape, the tape-covered spheres were
²⁴⁷ first wrapped with polyethylene film. Finally, liquid UV-curable plastic was applied as
²⁴⁸ the third and outermost layer and hardened using UV light. To maintain the sphericity
²⁴⁹ of the markers, crucial for radial reflection, the markers were continuously rotated dur-
²⁵⁰ ing the plastic curing process. Gloves were worn throughout the procedure to prevent
²⁵¹ fingerprints on the surface, which could degrade the reflectivity.

²⁵² Alternative methods for coating the screw-on spheres, such as retroreflective paints
²⁵³ and sprays, were explored, but they either did not provide a sufficiently strong retrore-
²⁵⁴ flective signal on the small surface of the sphere or lacked the durability required for
²⁵⁵ rodent experiments. After extensive testing, the finalized marker design demonstrated

256 strong signal detection by cameras, excellent durability, a damage-resistant surface,
257 and lightweight properties.

258 **3.5 Marker quality testing**

259 The quality of the retroreflective markers was tested before attempting to use them in
260 experiments. Individual markers were placed on a custom well-plate made from black,
261 non-reflective material in the motion capture arena, and tracking tests were conducted
262 using well-calibrated cameras. Each marker was subjected to random shaking for 20
263 seconds while being tracked. This process was repeated three times, with the well-plate
264 positioned differently for each trial.

265 During these "quality control recordings", the exposure setting for the motion
266 capture was reduced to half (25 μ s; frame rate kept at 300 fps) of the exposure used in
267 experimental conditions. Markers were deemed acceptable for experimental use only
268 if they were tracked without gaps throughout all three quality control trials. Markers
269 that did not pass the tests were discarded.

270 **3.6 Behavioral tracking using marker-based motion capture**

271 Motion capture recordings were conducted using the Qualisys Oqus 7+ camera sys-
272 tem (Qualisys, Gothenburg, Sweden; [44]). Standard 22 mm lenses were replaced with
273 40 mm lenses, optimized for small tracking volumes (focus distance during recordings:
274 39.5 mm; aperture: 2.8). Retroreflective markers were stroboscopically illuminated
275 with infrared LED ring lights attached to the cameras (exposure time: 50 μ s; frame
276 rate: 300 fps). Six cameras were positioned at 60° angles relative to each other, with
277 a slight downward tilt to optimize the capture of all markers. For the CLB task,
278 only four cameras were needed for tracking. Importantly, as the Qualisys motion cap-
279 ture cameras only produce marker coordinate data it is necessary to complement the
280 recordings with a well-placed conventional video camera to allow examination of the
281 non-tracked body parts.

282 To ensure the high quality of the triangulated positional data, the cam-
283 eras were regularly calibrated following standard procedures ([https://docs.
284 qualisys.com/getting-started/content/getting_started/running_your_qualisys_system/
285 calibrating_your_system/calibrating_your_system.htm](https://docs.qualisys.com/getting-started/content/getting_started/running_your_qualisys_system/calibrating_your_system/calibrating_your_system.htm)). Briefly, during calibration, the
286 spatial arrangement and lens properties of each camera are mathematically character-
287 ized to accurately reconstruct marker positions from multiple camera images through
288 triangulation algorithms (e.g., direct linear transformation methods; [45]). Calibration
289 was deemed successful when all cameras reported average residuals below 0.2 mm.

290 Although lighting and other environmental conditions do not directly affect marker
291 tracking accuracy because of dedicated infrared illumination, they can influence animal
292 behavior in open environments. Therefore, basic experimental precautions were taken,
293 including keeping ambient lighting conditions stable, minimizing noise, and restricting
294 personnel movements in the recording space. Importantly, the level of environmental
295 control needed may vary depending on how thoroughly animals are habituated to the
296 experimental conditions; in our experience, well-habituated animals exhibit stable and
297 naturalistic behaviors even under moderate changes in experimental conditions.

298 At the beginning of each recording, mice were placed in the arena used in training
299 period to confirm that all markers are clearly visible to at least 3 cameras using
300 the experimental recording parameters (300 fps with 50 μ s exposure time). After
301 completion of an experimental day, the marker trajectories were manually labeled
302 using default settings in QTM software (Qualisys, Gothenburg, Sweden; 2022 version)
303 and exported to MATLAB for further analysis. Animations of 3D marker position
304 reconstructions shown in the Movies are generated in the QTM software and exported.
305 The final Movies were compiled in DaVinci Resolve 19 (Blackmagicdesign, Fremont,
306 CA, USA).

307 **3.7 Gap filling and glitch removal**

308 Minimal post-processing was applied to marker trajectories only when necessary to
309 ensure data continuity for computational analysis. Short gaps (shorter than 50 frames
310 (~ 165 ms)) were bridged using linear interpolation, producing continuous trajectories
311 essential for calculations requiring uninterrupted data (e.g., windowed speed estima-
312 tion). Longer gaps, which occurred rarely, were excluded from subsequent analyses to
313 avoid introducing artifacts. Importantly, gap-filled sections were not used in analyses
314 of kinematic features such as step heights.

315 To address occasional short "jitter"— sharp, transient deviations caused by posi-
316 tional reconstruction ambiguity — a simple algorithm was employed. Jitter events were
317 defined as localized changes that exceeded 0.05 mm in peak prominence and lasted
318 for no more than three frames (~ 10 ms). The affected data points, along with their
319 immediate neighbors, were replaced with interpolated values to restore the continu-
320 ity of the trajectory. This process ensured that only clearly erroneous and short-lived
321 artifacts were corrected, preserving the integrity of the overall trajectory.

322 **3.8 Motion capture performance quantification**

323 The accuracy and reliability of the motion capture system were evaluated using three
324 key metrics: marker visibility, residuals, and positional error. These measures collec-
325 tively define the system's accuracy and robustness in reconstructing 3D trajectories
326 from markers on freely-behaving animals.

- 327 • Marker visibility (Figure 2c-e) quantifies the percentage of frames in which each
328 marker is successfully detected during a recording session. High visibility across
329 frames indicates consistent detection and tracking of markers, ensuring reliable
330 trajectory data.

- 331 • The residuals (Figure 2f) are generated by Qualisys QTM software and represent the
 332 average differences between the 2D marker rays that contribute to the reconstruction
 333 of a single 3D point ([46]).
- 334 • Tracking error magnitude (Figure 2g) was calculated for each pair of markers based
 335 on the absolute frame-by-frame differences between the distance measured between
 336 pairs of markers and the known distance between them. Assuming the two markers
 337 contribute equally to the error, the per-marker error was estimated as half of the
 338 pairwise error.

339 3.9 Kinematic measurement explanations and definitions

- 340 • General Locomotion Tracking (Figure 3): The midpoint between the two hip markers
 341 was used as a reference point for tracking general locomotion in the arena. Frame-
 342 by-frame speed of this point was calculated based on the 3D displacement distance
 343 over one second. For CLB and TRM tasks, displacement was calculated relative to
 344 the surface movement, which was tracked using markers attached to the edges of
 345 the wheel and treadmill belt. To detect the onset of locomotion, the velocity of the
 346 hip center point was calculated using displacement over 100 frames (~ 300 ms) for
 347 improved temporal resolution. "Locomotory episode" was defined as periods where
 348 the mouse moved faster than 40 mm/s for a minimum of 100 frames, allowing for
 349 brief dips below the threshold (up to 50 frames (~ 165 ms)) which corresponds to
 350 directed fast speed walking (as opposed to slow stepping in place).
- 351 • **Motion index (MI)** (Figure 4) was calculated as the average speed of all
 352 markers, based on the 3D displacement distance over 10 frames (~ 33 ms). This
 353 metric provided a comprehensive measure of whole-body movement, capturing both
 354 locomotory and non-locomotory activity.
- 355 • **Step detection** (Figures 5, 6, 8) relied on the vertical movement of the ankle
 356 marker during continuous locomotion during the TRM task. Swing periods were

357 defined as the intervals between consecutive minima in the vertical trajectory. For
358 OF and CLB tasks, swing definitions were based on ankle speeds calculated over
359 30-frame (~ 100 ms) intervals. Swing start and end points were identified by detect-
360 ing acceleration and deceleration peaks flanking high-speed ankle trajectories. This
361 method addressed challenges arising from non-orthogonal ankle movements and was
362 grounded in the principle that locomotory steps generate propulsion, which must
363 involve a distinct acceleration event. During CLB and TRM tasks, ankle speed was
364 calculated relative to surface motion, tracked using rim- or belt- attached markers.

365 **3.10 Kinematic step measure definitions:**

- 366 – **Duration** is measured from the start to the end of a swing period, with the
367 endpoint defined as the conclusion of the ankle deceleration phase in open field
368 and climbing.
- 369 – **Mean and maximum ankle speeds** are calculated for each ankle in each mouse
370 by averaging the mean or maximum frame-by-frame speeds observed during swing
371 periods.
- 372 – **Swing height** definition depends on the locomotion context. For horizontal loco-
373 motion (OF and TRM), swing height is the maximum vertical extent of the swing
374 trajectory. During CLB task, swing height is defined as the amplitude along the
375 second principal component of the 3D trajectory to account for the variable body
376 angles around the wheel.
- 377 – **Swing distance** refers to the Euclidean distance between the ankle positions at
378 the start and end of the swing.
- 379 – **Swing trajectory length** represents the total distance the ankle travels in 3D
380 space between the start and end of the swing.

381 **3.11 Tremor analysis:**

382 Tremor analysis was conducted using Fourier decomposition to construct the power
383 spectrum within the range of 6–18 Hz. To reduce noise, spline interpolation with
384 an automatically selected smoothing factor was applied. Tremor boundaries were
385 identified using two complementary strategies: (1) derivative noise analysis, with a
386 threshold set at 10% of the maximum derivative value, and (2) detection of local
387 maxima and minima if the derivative strategy was unsuccessful.

388 Tremor amplitude was quantified from trajectories filtered within the individual
389 tremor frequency bands identified for each marker. The Hilbert transform was
390 applied to compute the instantaneous amplitude from the modulus of the analytic
391 signal. Then these amplitudes were averaged across windows, axes, and markers for
392 statistical analysis.

393 Correlations between the instantaneous phases and amplitudes were derived from
394 the Hilbert transform for all combinations of axes and markers. This analysis was
395 used to identify the directional synchronization of oscillations within individual
396 markers and across multiple markers.

397 **3.12 Data analysis**

398 For grouped animal results, data are presented as mean + standard error (SEM)
399 and analyzed using a one-way or two-way analysis of variance (ANOVA) or paired
400 t-student test as appropriate. We did not exclude any data. In case of missing val-
401 ues, data were analyzed by fitting a mixed model, rather than by repeated measures
402 ANOVA. Dunnett's or Tukey post hoc comparisons were used. To examine the overall
403 performance of motion capture irrespective of the variability between animals (Figure
404 2), we pooled all frames and markers across all animals, separating the data into loco-
405 motory and non-locomotory frames. We used the non-parametric Mann-Whitney U
406 test (ranksum) for comparisons because the data did not meet normality assumptions.

⁴⁰⁷ Differences were considered significant at the level of $p < 0.05$. Statistical analysis was
⁴⁰⁸ performed with GraphPad Prism version 9.00 (San Diego, CA) or Matlab (ver. 2024a,
⁴⁰⁹ Mathworks, Natick, MA) ran on MacOS Sonoma 14.4.1.

⁴¹⁰ **4 Results**

⁴¹¹ **4.1 Realization of reliable long-term motion capture tracking**
⁴¹² **in mice**

⁴¹³ Figure 1 shows the arrangement of the motion capture recording environment (a, b;
⁴¹⁴ inset shows a close-up of a mouse wearing the retroreflective markers during a record-
⁴¹⁵ ing session), our chosen marker placements on a mouse, and an example frame with
⁴¹⁶ 3D reconstruction of the markers (c; see Movie 1, [6.1](#)). Six Qualisys Oqus 7+ cam-
⁴¹⁷ eras (Qualisys, Gothenburg, Sweden) are positioned around the experimental arena
⁴¹⁸ with a slight downward tilt and a 60-degree angle between each neighboring camera.
⁴¹⁹ Notably, adding more cameras does not benefit tracking performance unless there are
⁴²⁰ occlusions caused by task-specific equipment or image acquisition parameters are set
⁴²¹ suboptimally. Importantly, as the motion capture cameras only generate marker tra-
⁴²² jectories by means of on-board coordinate triangulation without saving video images,
⁴²³ an video camera (Miqus Hybrid, Qualisys, Sweden; 85 fps) is synchronized with the
⁴²⁴ motion capture system to provide a conventional record of the experiment. Mice are
⁴²⁵ thoroughly habituated to the experimental room and arena to minimize the effects of
⁴²⁶ stress on behavior (see Methods, [3.3](#)).

⁴²⁷ The foundation of the marker implant is a barbell-shaped stainless steel piercing
⁴²⁸ with screw-on spheres, originally intended for human skin decoration purposes. 18–20G
⁴²⁹ gauge piercings with 6, 7, and 8-mm-long shafts are used as appropriate for each body
⁴³⁰ part. The shafts weigh between 55.18 ± 0.26 mg (6 mm) and 69.38 ± 0.26 mg (8
⁴³¹ mm); the bare screw-on spheres weigh 94.54 ± 1.52 mg. For preparing markerheads

432 for motion capture use, the spheres (Figure 1 d) are covered with thin retroreflective
433 tape strips and polyethylene film, before coating them with liquid ultraviolet light-
434 curable plastic (final weight of retroreflective sphere: 239.37 ± 2.43 mg; see Methods
435 for full construction details). During the implantation procedure performed under
436 isoflurane anesthesia, small holes are punctured at key locations on mouse skin to
437 allow subcutaneous threading of the barbell piercing. The weight of the 10 uncoated
438 piercings worn by mice daily in this study was 1.2–1.3 g, amounting to not more
439 than 5–7 % of mouse body weight. The natural process of skin healing leads to secure
440 attachment of markers for extended use, and marker loss does not occur within the
441 first 3 months after implantation.

442 At the beginning of each recording, the steel spheres are exchanged for the larger
443 retroreflective markerheads. As the animals are thoroughly habituated to behavior
444 while wearing the larger markerheads, they do not display any discomfort. Notably,
445 while the total weight of the retroreflective markers (approx. 3 g) can reach 12% of
446 the mass of a 25 g mouse, the distribution of the weight across body parts suggests
447 the effort is not greater than that of many commonly-used head-mounted miniature
448 microscopes ([47]).

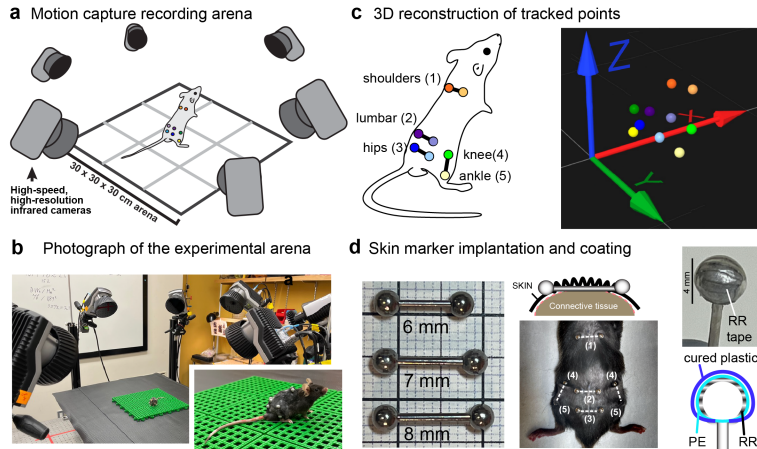


Fig. 1 Realization of MBMC in mice using barbell-shaped underskin marker implants. **a**, schematic of the motion capture recording set up; for actual scale see photograph in **b**. Inset shows a close-up of a mouse wearing retroreflective markers during a recording session. Note the relaxed posture of the animal despite absence of enclosure. **c**, schematic and labeling of marker positions used in this study (left) and a 3D reconstruction of marker positions from the QTM software. **d**, construction and attachment of skin marker implants. Three different lengths of barbell piercings were used as most fitting for a given body part (left). The shaft of the barbell piercing is inserted through and under the skin (middle). During motion capture recordings, the stainless steel 3 mm spheres of the piercings are replaced with 4 mm spheres that have been covered with retroreflective (RR) tape, polyethylene (PE) plastic film and coated with UV-cured plastic (right).

449 4.2 Performance of marker-based motion capture performance 450 in freely moving mice

451 An ideal motion capture methodology would allow precise, accurate and robust track-
452 ing of desired anatomical keypoints over extended periods (weeks) during naturalistic,
453 three-dimensional behavior with no need for extensive post-processing or missing data
454 inputation. The performance of the capture should be consistent regardless of the posi-
455 tion of the subject within the recording volume (e.g., distance to the recording area
456 borders) or behavioral state.

457 To validate the function of our motion capture system within these parameters, we
458 used a dataset that consisted of a cohort of 10 adult mice, wearing 10 markers, explor-
459 ing a square open field arena for one minute (three trials on different days; recorded
460 at 300 fps, resulting total 5400000 data points). Figure 2a shows the vertical trajec-
461 tories of all markers on the left side in a representative example of a complete recording,

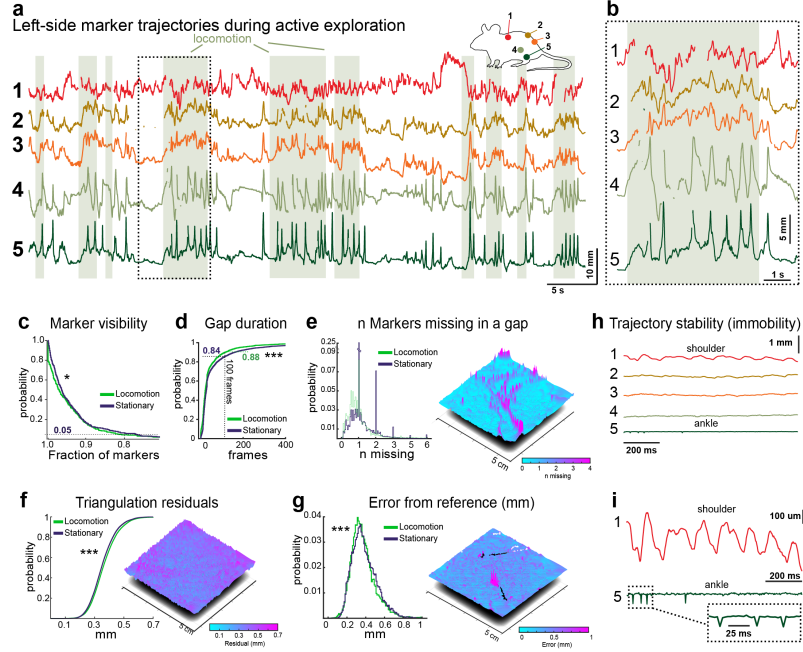


Fig. 2 Characterization of the robustness, precision and accuracy of motion capture tracking. **a**, representative example of raw vertical trajectories obtained from 5 markers on left side of the body. Schematic displays the color code for markers. Shaded green regions indicate periods when the mouse was locomoting. **b**, portion of trajectories indicated by dashed rectangle is shown in higher temporal resolution, displaying short duration of missing data. **c**, marker visibility shown as the probability that given fraction of markers is visible in a frame. The results are shown separately for locomotory and stationary periods. **d**, duration of tracking gaps shown as cumulative probability distributions for locomotory and stationary periods. Dashed lines highlight the probabilities that gap duration is less than 100 frames (~ 300 ms). **e**, probability for locomotory and stationary periods (left) and spatial distribution on the square recording arena (right) of missing markers counts, smoothed over 100 frames (~ 300 ms). The individual peaks in the right panel correspond to a single animal with somewhat worse marker quality. **f**, probability (left) and spatial distribution (right) of the triangulation residuals obtained from raw Qualisys tracking results. **g**, probability (left) and spatial distribution (right) of the tracking error, quantified as the difference from known reference distance between pairs of markers. **h**, representative vertical trajectories of all markers on one side of a mouse during a period of immobility. **i**, shoulder blade and ankle trajectories from **h** shown in higher spatial resolution. Note oscillations of 100–300 μm seen in shoulder marker possibly reflecting breathing movement. The dashed rectangle region from ankle marker is shown with expanded temporal resolution in the inset, showing unitary, 100- μm "glitches". *, p < 0.05; ***, p < 0.0001, Mann-Whitney U test.

462 without any post-processing besides trajectory labeling in the Qualisys QTM soft-
 463 ware. As seen in the segment shown extended in Figure 2 b, the gaps in trajectories
 464 were short and mostly appeared in a single trajectory at a time. The tracking reli-
 465 ability was consistently high (more than 80% markers were tracked in 95% of frames;
 466 Figure 2c). We noted that during passive immobility mice often sit in a posture that

467 partly occludes leg and shoulderblade markers leading to slightly more frequently
468 missing trajectories (median fraction of visible markers per frame 0.97 for both loco-
469 motory and non-locomotory frames, but 95th percentile 0.82 and 0.77 for locomotory
470 and non-locomotory frames, respectively; $p = 0.012$, Mann-Whitney U test). However,
471 especially during locomotion, long gaps were rare (median gap duration 22 and 27
472 frames (~ 73 and 90 ms); 95th percentile of gap durations 184 and 289 frames (~ 607
473 and 954 ms), in locomotory and non-locomotory frames, respectively; $p < 0.001$ (Mann-
474 Whitney U test); Figure 2d) and were contributed mainly by a single missing marker
475 (Figure 2e, left). Naturally, individual markers can become less visible if their surface
476 degrades leading to a situation where they can be less perfectly tracked throughout the
477 trial. These individual cases are easily identifiable as "paths" of poor tracking when
478 examining the spatial distribution of gaps during the experiment (Figure 2e, right).

479 A standard way of quantifying tracking precision is built on the residual tri-
480 angulation value, a measure of how precisely the 3D position of each marker can
481 be reconstructed ("triangulated"; [45]) from multiple camera views. As each camera
482 captures a 2D projection of the marker, triangulation combines these multiple 2D
483 images to estimate markers' 3D positions. The residual of triangulation represents the
484 discrepancy or error between the reconstructed 3D position and the underlying 2D pro-
485 jections. In our 6-camera setup, these triangulation residuals ranged between 0.2 and
486 0.6 mm during experimental recordings, with slightly lower performance during loco-
487 motion (median residual 0.36 and 0.35 mm; 95 % percentile bounds 0.53 and 0.51 mm,
488 for locomotory and non-locomotory frames, respectively; $p < 0.001$ (Mann-Whitney U
489 test); Figure 2f).

490 Furthermore, leveraging the fact that our marker pairs are placed at known dis-
491 tances between each other, we could estimate the real tracking accuracy that depends
492 on the size, visibility, and sphericity of the markers. Across all markers, the discrep-
493 ancy in the tracked distance between the pair of markers and their known distances

494 was also in the submillimeter range (median error 0.35 and 0.37 mm; 95 % percentile
495 bounds 0.63 and 0.64 mm for locomotory and non-locomotory frames; $p < 0.001$ (Mann-
496 Whitney U test); Figure 2g). These measurements indicate that even when used in the
497 challenging context of a moving mouse with hand-made markers, it is reasonable to
498 have confidence in submillimeter location accuracy not far from the device capability
499 reported for best-case scenarios [13].

500 In markerless tracking approaches, small high-frequency positional fluctuations
501 (“jitter”) arising from ambiguity among nearby pixels can complicate the analysis
502 of subtle behaviors, as these fluctuations could be misinterpreted as distinct events
503 (e.g. [22]). Although they can to an extent be removed from trajectory data in post-
504 processing, such cleaning may inadvertently remove real features of movement. In
505 contrast, the marker-based trajectories we recorded rarely exhibited such jitter, espe-
506 cially under well-calibrated conditions where markers remain visible from multiple
507 camera angles. As exemplified by the raw trajectories recorded during passive immobil-
508 ity periods (Figure 2h), jitter was minimal. Instead, the predominant subtle movement
509 observed was a low-amplitude (~ 8 Hz) oscillation of shoulder blade markers, possibly
510 reflecting respiration (Figure 2i, top trace). Ankle markers occasionally showed single
511 frame glitches of less than 100 μm (Figure 2i, bottom trace). Such minor artifacts are
512 straightforward to remove by simple interpolation, similarly to the handling of short
513 gaps.

514 Taken together, these assessments indicate that marker-based tracking on freely
515 moving mice can offer continuous, submillimeter precision tracking of anatomically
516 relevant markers with minimal data loss or jitter. This allows for confident use of its
517 output in subsequent analyses without further post-processing such as smoothing or
518 model fitting.

519 **4.3 Context-dependent behavioral disruption of general**
520 **locomotory parameters by cannabinoid receptor agonist**

521 To validate our method compared to established behavioral assays, our objective was
522 first to reproduce well-characterized behavioral alterations induced by CP55,940 (CP;
523 0.3 mg/kg), a cannabinoid CB1 and CB2 receptor agonist. Although tracking gen-
524 eral parameters such as animal position and speed can be adequately accomplished
525 with markerless or even simpler image-thresholding-based analysis (such as Bonsai-RX
526 (<https://bonsai-rx.org/> [48]), Ethovision XT (Noldus, Wageningen, The Netherlands
527 (<https://noldus.com/ethovision-xt>)), demonstrating these effects under our experi-
528 mental conditions ensures that marker implantation and lack of enclosure in the motion
529 capture setup do not obfuscate the well-established but subtle effect. To this end, we
530 assessed voluntary locomotion during open field (OF) exploration, and further added
531 two novel locomotory tasks: vertical wheel climbing (CLB), and treadmill running
532 (TRM; see examples in Movies 2, 3, and 4 [6.2](#), [6.3](#), [6.4](#)). As illustrated in Figure
533 [3a](#), we monitored the position and instantaneous speed of the midpoint of the hip
534 markers to quantify the total distance traveled during a trial (Figure [3b](#)), time spent
535 locomoting (Figure [3c](#)), and locomotion speed (Figure [3d](#)). Indeed, as expected and
536 previously demonstrated for the moderate dose of CP using conventional behavioral
537 apparatuses ([39, 40]), mice exhibited a slight inhibition of locomotion expressed as
538 a trend towards decreased distance traveled [$F(1, 15) = 4.122, p=0.060$] and signifi-
539 cantly decreased time spent locomoting [$F(1, 15) = 6.824, p=0.0196$]. There was no
540 effect on locomotion speed [$F(1, 23) = 0.02, p=0.89$]. Surprisingly, locomotion during
541 climbing was completely unaffected - distance traveled ($p=0.31$), time spent locomot-
542 ing ($p=0.51$) and speed ($p=0.94$) were not altered by CP administration, although OF
543 and CLB tasks were carried out within minutes of each other. Interestingly, CP signif-
544 icantly decreased the maximum speed at which mice were able to run on a motorized

⁵⁴⁵ treadmill, on average by 10 m/min, from 28 ±3.7 to 15±3.9 (mean± SEM) (t=4.33,

⁵⁴⁶ p=0.012).

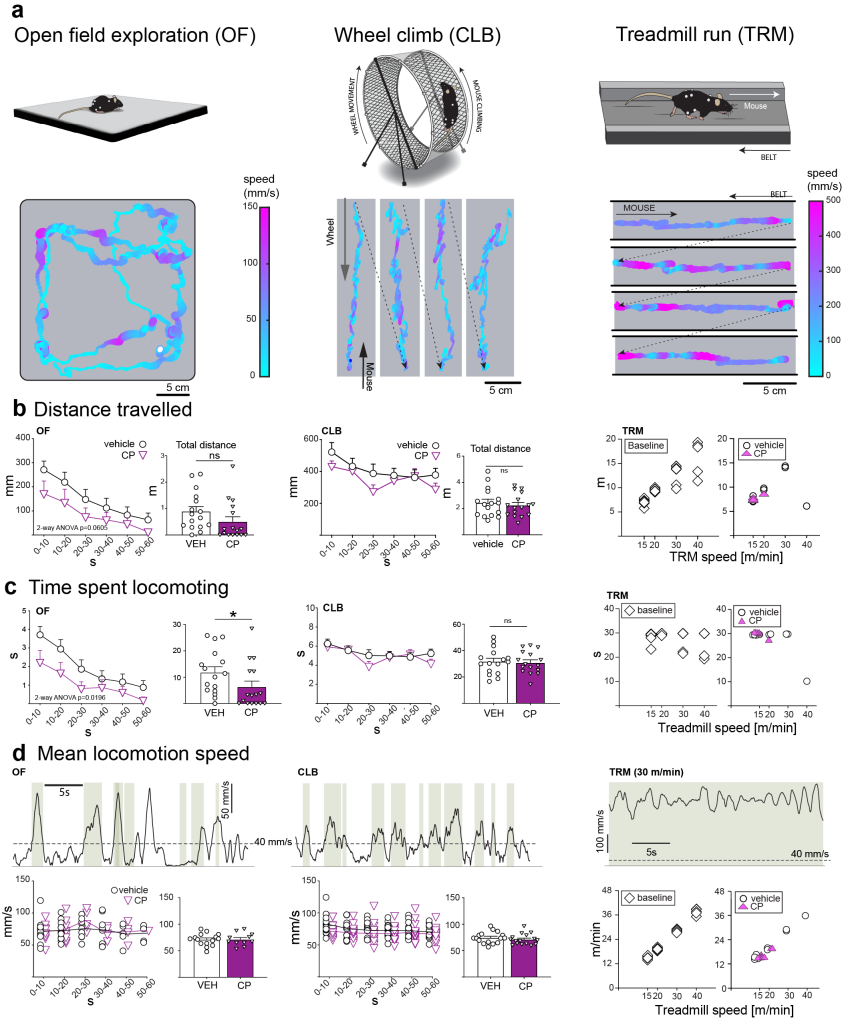


Fig. 3 Using motion capture to monitor general activity parameters in 3D environments. **a**, schematic description of the three locomotory behaviors used in this work (top panels) and representative example trials (bottom panels). Animal position is shown as the midpoint of hip markers, color-coded with speed. Position on wheel and treadmill is shown with respect to the moving substrate (wheel or treadmill band, respectively). **b**, effect of CP55,940 on distance travelled during full trials shown binned means of all animals + SEM (left panels) and as total values for full trials (right panels). For treadmill data, both baseline (no injection) and vehicle-injected groups are shown. **c**, top panels: representative trial speed profiles from the three behaviors. Shaded green regions denote periods when mouse was locomoting (mean speed higher than 40 mm/s, indicated by dashed line). **c**, bottom panels: binned means for individual animals speeds while locomoting (left panels) and mean locomotory speeds over whole trials (right panels), shown for vehicle and CP55,940 groups. * $p<0.05$ in paired t test. **d**, time spent locomoting shown binned (left panels) and over whole trials (right panels). Note that the only metric reaching statistical significance is time spent locomoting in the open field.

547 **4.4 MBMC provides additional resolution to activity**
548 **monitoring**

549 Although basic parameters such as mouse position and average speed within a 2D
550 environment — or even distance traveled on a climbing wheel — can be adequately
551 captured using simpler means, additional insights are gained through MBMC when
552 assessing small-amplitude movements across multiple markers.

553 As illustrated in Figure 4a, we define a "Motion Index" (MI) as the average instant-
554 taneous speed of all markers, providing a sensitive measure of subtle body movements.
555 Naturally, MI increases during locomotion and scales with the animal's speed. Impor-
556 tantly, MI also captures very small movements occurring during stationary periods,
557 such as grooming, sniffing, or minute postural adjustments, which can be informative
558 of the animal's behavioral state beyond overt locomotion alone ([49]) Importantly,
559 movements during stationary periods were extraordinarily small (mean marker dis-
560 placement over 10 frames (33 ms) in VEH: 0.6 ± 0.3 mm; CP: 0.29 ± 0.27 mm; $p <$
561 0.001, Wilcoxon rank-sum) and their reliable detection is necessary for differentiating
562 between groups.

563 Indeed, CP-treated mice exhibited consistently lower MI values throughout OF
564 trials ($[F(1, 15) = 12.71]$, $p = 0.0028$; Figure 4b). This decrease in MI was entirely
565 driven by suppression of movements during stationary periods (Figure 4c; $p = 0.025$
566 and 0.54 for changes in average stationary and locomotory MI, respectively), consistent
567 with unchanged locomotion speeds. In contrast, MI during the CLB task did not differ
568 significantly between CP- and vehicle-treated trials overall ($p = 0.27$; Figure 4d), nor
569 when comparing stationary and locomotory periods separately ($p = 0.22$ and 0.94;
570 Figure 4e). This reflects the tendency of mice to move and shift posture constantly
571 even during the brief climbing pauses (Figure 4; see Movie 3, 6.3).

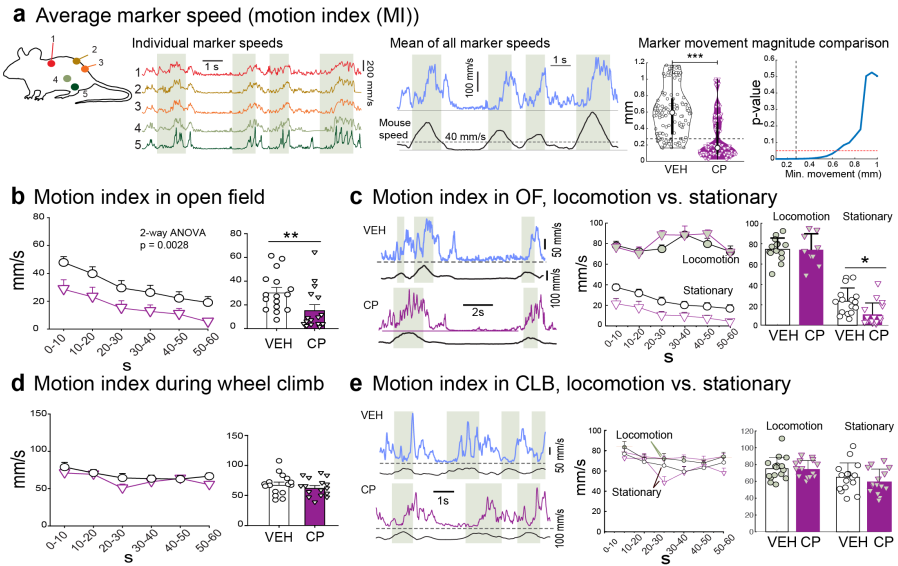


Fig. 4 Motion index (MI) resolves fine effects of CP55,940. **a**, construction of motion index as the average speed of all markers. Schematic of marker locations and their instantaneous speeds(left) and during a period consisting of locomotion (shaded areas) and immobility. Middle panel shows the average of all marker speeds over the same period (blue) and mouse speed (black). Rightmost panels compare the mean 2D magnitude of marker movement over 10 frames between VEH and CP groups (violin plots), as well as the effect of minimal detectable movement size on the distinction between the groups. Black dashed line denotes an estimated noise-floor (0.28 mm) based on projecting our 3D triangulation residual mean of 0.35 to 2D. Red dashed line denotes $p = 0.05$. ***, $p \leq 0.001$, Wilcoxon ranksum **b**, MI during open field exploration (OF). CP55,940 significantly decreases MI in 10-s bins (left) and in trial averages (left). ** $p < 0.01$ in paired t test. **c**, in OF, CP55,940 decreases MI during immobility periods. Left panel shows example MI and speeds of a mouse in a period of two locomotory episodes and an intervening period of immobility for vehicle (top) and CP55,940 (bottom) treated animals. Dashed line indicates MI=0. Middle panel: binned MI values for periods of locomotion and stationarity. Right panel: whole-trial means for locomotion and immobility. * $p < 0.05$ post hoc comparison. **d**, MI is not affected by CP55,940 during climbing, binned (left) or overall (right). **e**, no change in MI for either locomotion or time spent immobile during climbing. Panels as in c.

572 4.5 Ankle swing kinematics during fast treadmill running

573 Moving beyond the description of general whole-body locomotion parameters, we
 574 examined the 3D trajectories of hindlimb ankles during running on treadmill at dif-
 575 ferent speeds (see Movies 5 - 7 ([6.5](#), [6.6](#), [6.7](#)), for reconstructions with real-time and
 576 slowed-down framerates) to see if we could identify features specifically affected by
 577 CP administration. As shown in Figure 5a-b, individual steps were readily identifiable
 578 with relatively uniform waveforms that, with increasing treadmill speeds, decreased
 579 in amplitude but covered longer horizontal distances due to faster movements of the

580 limbs. Importantly, during slower running (15 m/min), the ankle moved at relatively
581 uniform speed, but faster running was associated with an increasingly sharp timing
582 of the peak ankle speed to match the contact with the treadmill (Figure 5 c) and the
583 ankle slowed during the swing peak and the downward swing phases.

584 In line with our observation that the mice were unable to run at high speeds after
585 CP administration, we found that their swing kinematics were also affected (Figure
586 5d). Comparison of kinematic measures between vehicle- and CP-treated mice running
587 at the lowest tested speed (15 m/min, the only speed CP-treated mice reliably ran)
588 revealed significantly decreased ankle swing height ($F (1, 3) = 39.00$, $p=0.0083$) as
589 well as a decrease in mean ($F (1, 3) = 22.96$, $p=0.017$) and maximum $F (1, 3) =$
590 10.26, $p=0.049$) ankle swing speed. There were no changes in the swing distance (p
591 = 0.20). Intriguingly, we noticed a slight but significant change in the distribution of
592 peak ankle speed timing so that the down-swing speed peak shifts closer to the swing
593 peak (median peak speed timing 0.08 and 0.06 s after swing peak for vehicle and CP
594 groups; $p <0.0001$, Mann-Whitney U test; Figure 5e).

595 4.6 Ankle kinematics during voluntary locomotion in the open 596 field

597 Behavioral models commonly used to examine mouse limb kinematics include forced
598 locomotion on a treadmill [50, 51] or in narrow walkways [50, 51]. Restricting move-
599 ment into one direction greatly simplifies motion tracking and allows collecting
600 supposedly uniform step trajectories during a short experimental trial. However, the
601 emotional and motivational state of the mouse can modulate motor behavior[52], and
602 the kinematic characteristics important for self-driven voluntary locomotion might be
603 masked if locomotion is forced or restricted.

604 Thus, since we had observed that CP55,940 caused a subtle suppression of loco-
605 motor activity in the open field (OF; Figure 3), we wondered if the kinematics of the

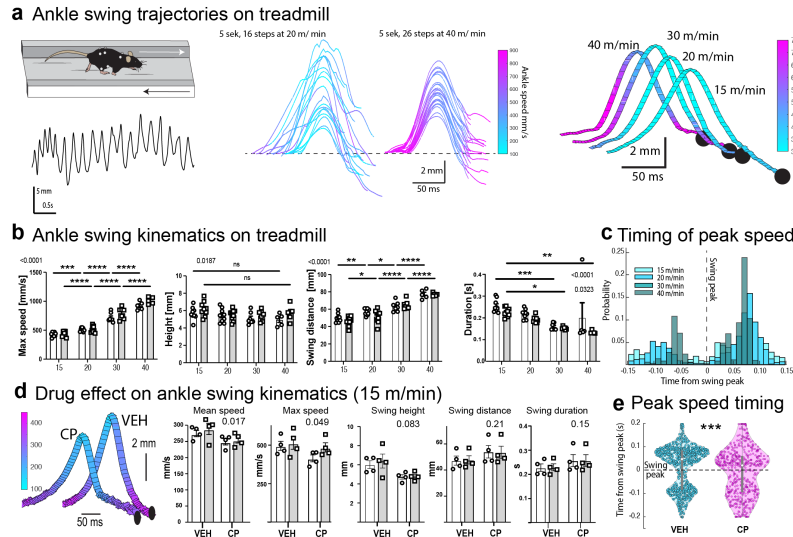


Fig. 5 Hindlimb swing kinematics during treadmill running. **a**, left: schematic and a representative example of vertical ankle trajectory during continuous treadmill running at 20 m/min. Middle: individual swing trajectories color coded for instantaneous speed, for 20 and 40 m/min running. Right: average ankle trajectories for swings during running at different speeds. Color indicates instantaneous speed. Trajectories are graphically arranged for visualization. **b**, ankle swing features for all mice running at all speeds. From left: maximal swing speed, swing height, horizontal swing distance and swing duration. White and gray data represent left and right legs, respectively. 2-way ANOVA: factors speed x leg side - first number indicates p value of speed factor and second number p value of leg side factor. * $p<0.05$, ** $p<0.01$, *** $p<0.001$, **** $p<0.0001$ post hoc comparison ($n=9$). **c**, timing of highest ankle speeds with respect to vertical swing peak time (dashed line) shown for all speeds examined. Regardless of running speed, ankles move fastest when close to the treadmill. **d**, effect of CP55,940 (0.3 mg/kg) on swing kinematics. Leftmost panel shows average swing trajectories for a representative mouse in vehicle and CP conditions. Color coding and graphical arrangement as in panel a. Bar graphs show swing kinematics for 15 m/min running speed; white and gray data correspond to left and right legs. 2-way ANOVA: factors treatment x leg side ($n=6$), p value indicates effect of treatment. **e**, CP55,940 affects the timing of peak ankle speeds during 15 m/min treadmill running. **** $p<0.0001$, Mann-Whitney U test.

606 OF steps would be affected similarly to those seen in the treadmill trials (decrease in
607 speed and swing height).

608 Voluntary exploratory locomotion in mice is inherently variable and consists of
609 periods of forward movement (locomotory episodes) and intermittent periods of other
610 activities such as grooming or postural changes. Importantly, many of such nonloco-
611 motor behaviors involve limb movements, and as a result it is not possible to reliably
612 detect locomotor steps by vertical motion alone. Therefore, we constructed a more

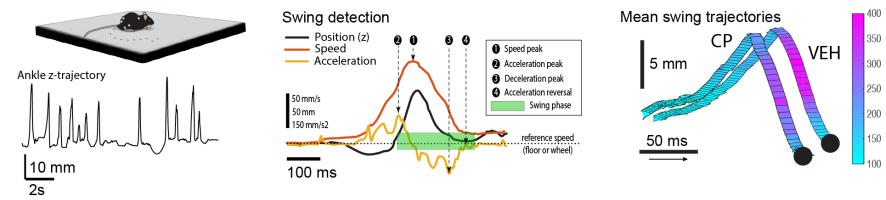
613 context-appropriate locomotory step detection procedure (Figure 6a, left and mid-
614 dle panels). Briefly, we delineate locomotory ankle swing periods by acceleratory and
615 deceleratory events rather than position. As shown for an example animal in Figure 6a
616 (rightmost panel), exploratory ankle swings were characterized by a sloping upward
617 motion followed by a rapid ankle drop, resulting in an asymmetric trajectory that was
618 surprisingly unaffected by the administration of CP55,940. Examination of the kine-
619 matic parameters of the swing in all animals (Figure 6b) confirmed the observation
620 that a moderate dose of cannabinoid agonist did not lead to a decrease in the speed,
621 distance or duration of the ankle swing. However, we noticed a decrease in the average
622 heights of the left ankle swings, possibly reflecting a drug-induced bias in behavioral
623 lateralization.

624 Thus, we conclude that the slight locomotory inhibition in the OF task induced
625 by CP is mostly expressed as a suppression of activity during non-locomotory periods
626 and somewhat increased reluctance to move, with very limited effects on locomotory
627 kinematics.

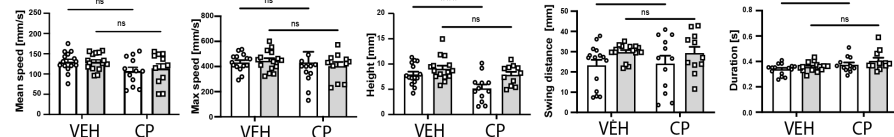
628 **4.7 Ankle kinematics during voluntary wheel climb locomotion**

629 Comparison of general locomotion parameters during OF and CLB tasks under CP
630 treatment revealed a noteworthy and novel finding: there was no suppression of loco-
631 motion in CLB task (see Figure 3). To examine whether ankle kinematics were affected
632 by CP during CLB, we detected ankle swings using the same criteria as for OF, with
633 the difference that speed and acceleration were calculated with respect to the wheel
634 movement, tracked using markers attached to the rim. Furthermore, the swing "height"
635 was defined perpendicularly to the wheel (Figure 6c). Given that none of the general
636 locomotion parameters were affected during CLB, we were surprised to find that mean
637 ($F (1, 15) = 7.66, p=0.014$) and maximum ($F (1, 17) = 15.66, p=0.001$) ankle speeds

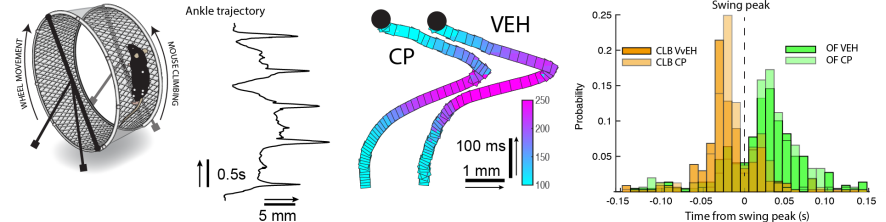
a Ankle swing trajectories during open field exploration



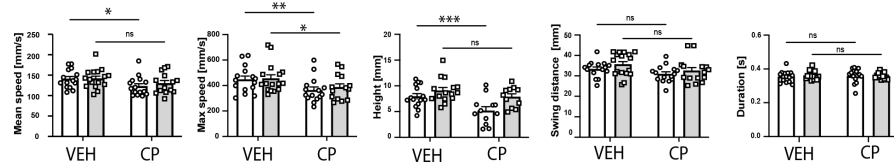
b Ankle swing kinematics during open field exploration



c Ankle swing trajectories during wheel climbing



d Ankle swing kinematics during wheel climbing



e Peak velocity timing

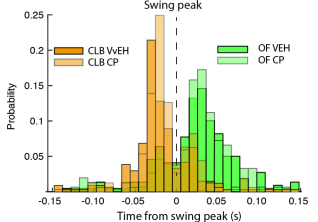


Fig. 6 Hindlimb kinematics during intermittent locomotion. **a**, left: schematic and representative ankle trajectory during a period of voluntary OF exploration. Note variability of movements. Middle: schematic describing step detection in OF and CLB tasks. Right: average ankle trajectories for a representative mouse exploring the OF in vehicle and CP conditions. Color coding represents instantaneous ankle speed. Trajectories are arranged graphically for easy visualization. **b**, summary of ankle swing kinematics on OF under vehicle and CP conditions. White and gray bars refer to data from left and right ankles, respectively. **c**, left: schematic and representative ankle trajectory during wheel climbing, shown in plane perpendicular to wheel and corrected for wheel movement. Time axis runs upwards. Right: average ankle swing trajectories from a representative mouse under vehicle and CP conditions, color coded for instantaneous speed. Time axis runs upwards. **d**, timing of ankle speeds with respect to swing peak timing differs in OF and CLB tasks (green vs. orange bars). CP does not affect timing compared to vehicle condition (weak vs. strong colors). **e**, summary of ankle swing kinematic measures for vehicle and CP conditions. White and gray data represent left and right ankle measurements, respectively. Abbreviations: CP, CP55,940 (0.3 mg/kg); VEH, vehicle; OF, open field; CLB, climbing. 2-way ANOVA, factors treatment x leg side: *p<0.05, **p<0.01, ***p<0.001 in post hoc comparison (n=16).

decreased significantly in the CP-treated group (Figure 6d) compared to vehicle. Furthermore, the swing height ($F (1, 15) = 27.17, p=0.0001$) was significantly reduced,

640 asymmetrically in the left leg ($F(1, 15) = 16.56$, $p=0.001$), as was also observed in the
641 OF and treadmill data (Figure 5). There was a small decrease in swing distance ($F(1,$
642 $16) = 4.78$, $p=0.044$) but duration of the swing was not affected ($F(1, 15) = 0.025$,
643 $p=0.87$).

644 Finally, we compared the timing of peak ankle speed with respect to the ankle swing
645 period during horizontal or vertical voluntary locomotion, as was done for treadmill
646 locomotion (Figure 6e). Although CP did not alter ankle speed timing in OF or CLB
647 tasks, we found a clear difference between the three locomotor contexts. First, in
648 contrast to the sharp timing of the high-speed motion at the onset of the swing on the
649 treadmill, the fastest ankle movements occurred just after and before the swing peak
650 for OF and CLB, respectively. These differences reinforce the notion that even though
651 all three contexts involve locomotion, they may involve distinct motor programs of
652 the limb, potentially leading to different responses to pharmacological interventions.

653 4.8 Harmaline tremor

654 Going beyond what previously has been possible in the realms of mouse kinematic
655 tracking, we aimed to test whether MBMC could be used to investigate very fine move-
656 ments such as tremor. Pathological tremor is a symptom of Parkinson's disease (PD)
657 [53] and analysis and decomposition of its kinematic characteristics using accelerome-
658 ter data from wearables or even smartphones [54, 55] show promise for the diagnostic
659 process for differentiating PD [56, 57] from essential tremor (ET; [58]). Despite the
660 clear need for fine measurement of tremor in animal models, current approaches are
661 rather crude and limited to methods such as quantifying tremor frequency band
662 fluctuations reported by force plates [59]. Among others, questions related to body-
663 part specificity and tremor lateralization in animal models have not been possible to
664 investigate.

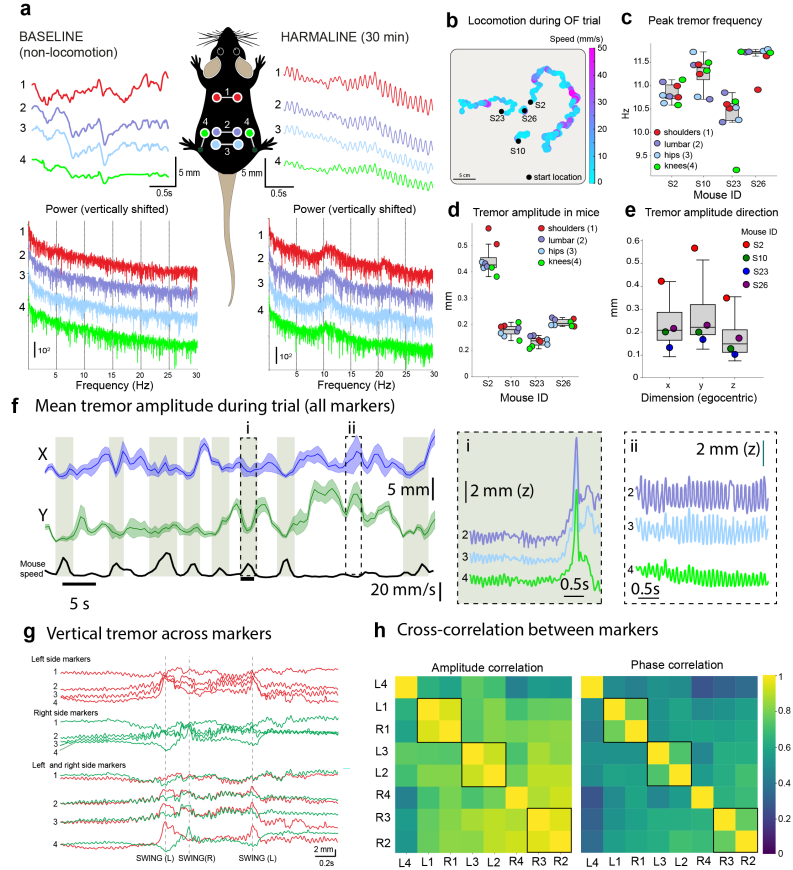


Fig. 7 Motion capture of full-body harmaline tremors. **a**, unilateral, vertical trajectories of back, hip, lumbar and knee markers from a mouse before (left) and after harmaline administration, during a period of passive immobility. Bottom panels show power spectrum densities for the same markers; the traces are vertically shifted to easier visualization. **b**, movement in the open field arena of the 4 mice examined after harmaline administration. Color coding indicates locomotion speed. **c**, peak tremor frequency for individual markers (colored symbols) on the 4 mice (box plots). **d**, mean tremor amplitude for individual markers (colored symbols) on the 4 mice (box plots). **e**, mean tremor amplitude for individual mice (colored symbols) in the three dimensions (box plots, in egocentric coordinates). **f**, tremor trace shows mouse speed. Shaded green rectangles indicate periods of movement faster than 10 mm/s. Panels i and ii show the vertical trajectories of hip, lumbar and knee markers during preparation to a step (i) and passive immobility (ii). **g**, vertical trajectories of the markers during a sequence of steps. Traces on top are arranged by side on top, vertically aligned at the peak of the first swing (dashed lines). Bottom traces are arranged by marker position to highlight precise phase-locking. Traces are vertically aligned at first swing start. **h**, amplitude (left) and phase (right) cross-correlation matrices for shoulder blades, lumbar spine, hip and knee markers in all 4 animals (indicated by numbers as in panel a). L and R refer to left and right sides. Rectangles highlight 3 pairs of markers with high correlation.

665 To examine the possibility of using MBMC for decomposing body tremors across
666 body parts, we tracked 4 pairs of markers (shoulder blades, lumbar spine, hips and

667 knees) in 4 mice freely behaving in the open field after administration of tremorgenic
668 harmaline (20 mg/kg; [60]). Due to the posture and very low mobility of the harmaline-
669 treated animals, ankle markers were often not visible and were not tracked in this
670 analysis. As shown in Figure 7a, the tremors are visible in all tracked markers (top
671 panels) with a clearly identifiable peak at "classic" frequencies (8-12 Hz; [42, 61–63], see
672 Movie 8, 6.8). All mice displayed severe suppression of locomotion (Figure 7b), so that
673 two of them (S10 and S23) did not take any forward steps during the recording despite
674 exhibiting other stationary behaviors such as grooming. The mean peak of the tremor
675 frequency varied more between animals than among the markers on a single animal
676 (ANOVA values for markers in each animal, $F = 0.181 - 5.41$, $p = 0.01-0.84$; comparing
677 the 4 animals in the experiment, $F = 18.61$, $p < 0.0001$; Figure 7b). Amplitude of the
678 tremor varied between markers on an animal likely reflecting differences in movement
679 range, and was overall higher in the individual that was locomoting most (S2; Figure
680 7d; ANOVA for markers in each animal, $F = 7.65-22.14$; for the 4 animals in the
681 experiment, $F = 138.03$, $p < 0.0001$). Across animals, the vertical-directed movement
682 of tremor was slightly but insignificantly smaller than horizontal (Figure 7e; $F = 0.51$,
683 $p = 0.62$).

684 The higher tremor amplitude in the mouse that was moving the most prompted
685 us to investigate whether the tremor would be specifically enhanced during periods of
686 increased activity. Figure 7f shows data from mouse S2 that showed periods of motility.
687 The movement was always slow, never reaching our conventional forward displacement
688 threshold of 40 mm / s as a definition of locomotion, and the locomotor episodes (> 10
689 mm/s; indicated by green shading in Figure 7f) consisted of not more than 2-3 steps
690 at most. However, in this individual, the tremor was in fact suppressed during forward
691 movement and reached highest amplitudes during periods of stillness (see insets i and
692 ii in Figure 7f showing vertical trajectories of markers lumbar, hip, and knee).

693 Next, we examined to what extent the tremors are correlated across the different
694 parts of the body. To our surprise, we found a very clear phase and amplitude corre-
695 lation, not only between the left and right sides of the animal that could be explained
696 to some extent by the physical connection between left and right markers (Figure 7g,
697 top traces) but also along the entire rostro-caudal "chain" of markers (from shoulders
698 to knees; Figure 7g, bottom traces). In fact, in the four animals, a positive correla-
699 tion was found in both amplitude (Figure 7 h, left) and phase (Figure 7h, right) for
700 all markers, including distant pairs (e.g. left shoulder vs. right hip). The whole-body
701 correlation of tremor is particularly well visible in slow-motion videos of tremoring
702 animals (see Movie 9, 6.9).

703 4.9 Ankle kinematics after harmaline administration

704 As the harmaline-treated mice did not locomote sufficiently in the open field nor on
705 the climbing wheel (Movies 10 and 11, 6.10,6.11), we examined limb kinematics on
706 treadmill on which the mice were able to maintain instantaneous advancing speeds
707 over 40 mm/s on up to 10 m/min treadmill speed (Figure 8a; Movie 12, 6.12). Even
708 though their capacity for locomotion was significantly lower than that of the same
709 animals without drug administration or with CP administration (Figure 8 bi-ii), the
710 results suggest that the lack of locomotion in OF under harmaline could be caused by
711 aversion to movement rather than a fundamental inability to locomote. Nevertheless,
712 some of the harmaline-treated mice were unable to continue locomotion for the entire
713 duration of the 30-s trial (Figure 8 biii-iv)), suggesting that exercise was unusually
714 exhausting.

715 The hindlimb trajectories of harmaline-treated mice showed clear oscillations
716 before and after swing movements (Figure 8c). Comparison with control groups was
717 not feasible due to the refusal of untreated mice to maintain steady locomotion on
718 treadmill speeds below 15 m/min. However, we noticed that the ankle movements

719 leading to swing were very slow (cyan coloring in trajectories in Figure 8c, d [64, 65].
720 Furthermore, while maximum ankle speeds occurred robustly during the swing phase
721 when locomoting on slow treadmill (1-5 m/min), at the highest speed (10 m / min)
722 the timing of peak ankle speed was spread throughout the swing phase (Figure 8e).
723 This was in contrast to the timing of the maximum ankle speed in the control tread-
724 mill trials (Figure 5c), possibly indicating that the tremor interferes with fine limb
725 control during locomotion. This disruption of ankle speed timing aligns with the obser-
726 vation that mice could not increase ankle speeds or heights when the treadmill speed
727 increased from 5 m/min to 10 m/min (Figure 8 f), which could lead to inefficient
728 locomotion and eventual trial failure.

729 5 Discussion

730 In this study, we establish that MBMC can track full-body kinematics in freely mov-
731 ing mice with submillimeter accuracy. By carefully optimizing marker construction,
732 placement, and camera positioning, we obtained high-resolution trajectories that accu-
733 rately capture both fine- and large-scale movements without the need for extensive
734 post-processing. This approach complements markerless technologies, which excel in
735 situations where marker attachment is infeasible (e.g., wild animals), high-throughput
736 recordings are required, or pose estimates provide sufficient insight.

737 Importantly, markerless methods are inherently constrained to tracking movements
738 that align with their training data, possibly limiting their ability to uncover novel fea-
739 tures even under constant data acquisition conditions. In contrast, MBMC directly
740 measures marker positions, generating data independent of prior models or datasets,
741 enabling the detection of previously unknown motion patterns. This independence
742 eliminates the need for training datasets or model retraining, making MBMC partic-
743 ularly valuable for applications requiring the reliable capture of subtle motions, such

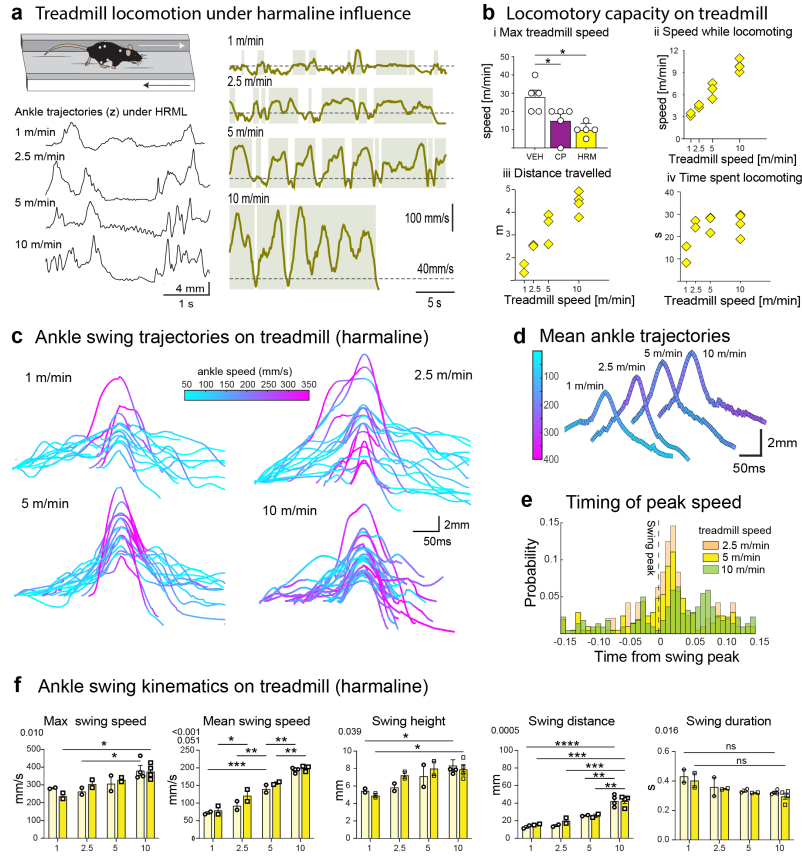


Fig. 8 Ankle swing kinematics during treadmill locomotion under harmaline-induced tremor. **a**, left: schematic and representative vertical trajectories of ankle during running on treadmill at different speeds. Right: mouse speed during full 30-s trials. Green shaded areas indicate periods of faster than 40 mm/sec, indicated by dashed line. During fastest speed, the mouse was not able to continue locomoting for the full trial. **b**, locomotory capacity on treadmill. **i**, comparison maximal speeds reached by mice in vehicle, CP and harmaline conditions; each marker represents a single mouse. **ii-iv**, general locomotory parameters on treadmill at 1 - 10 m/min speeds. **c**, example vertical trajectories of ankle swings at different speeds from a single mouse. Color indicates instantaneous ankle speed. **d**, mean ankle trajectories for the same mouse. Color indicates instantaneous ankle speed. Traces are arranged graphically for visualisation. **e**, timing of peak ankle speed with respect to ankle swing peak (dashed line) with the three highest speeds. **f**, summary of ankle swing kinematic measures for all animals during treadmill locomotion. Light and dark-colored data corresponds to left and right ankles, respectively. 2-way ANOVA, factors speed x leg side: * $p < 0.05$, ** $p < 0.01$, *** $p < 0.001$, **** $p < 0.0001$ in post hoc comparison ($n=6$).

as tremor, or the precise quantification of low activity levels (e.g., the "motion index" in this study).

746 In the following, we first address key methodological considerations and then dis-
747 cuss how our proof-of-concept pharmacological experiments illustrate the potential of
748 MBMC to detect motor alterations in different locomotory contexts.

749 **5.1 Realization of marker-based mouse motion capture using
750 skin-implantable markers**

751 A core challenge with markerless motion tracking is its reliance on fully annotated
752 training data sets and its susceptibility to occlusions, variable lighting, and general-
753 ization issues across individual animal differences. Marker-based tracking avoids these
754 limitations by removing the need for background subtraction and explicitly defining
755 the points to be tracked. This removal of ambiguity directly yields clean, ready-to-
756 use 3D data, eliminating the need for complex and largely opaque post-processing
757 pipelines.

758 In theory, the quality of MBMC data is entirely determined by the physical dimen-
759 sions of markers and the optical characteristics of cameras. Thus, in the absence of
760 noise, the process of reconstructing the marker positions by triangulation is straight-
761 forward [66, 67]. However, achieving such a level of tracking in mice presents unique
762 challenges, primarily due to their tendency to destroy or remove foreign objects on
763 their skin. This limitation has confined marker-based studies in mice to brief record-
764 ings, requiring frequent marker replacement, which can lead to inconsistent marker
765 positioning and unnecessary stress to the animal. Furthermore, the looseness of mouse
766 skin complicates accurate tracking of the underlying body structures using skin-
767 top markers ([68]). Although these issues are somewhat less pronounced in larger
768 rodents, such as rats ([38, 69]), mice remain the most widely used vertebrate mod-
769 els in systems and behavioral neuroscience ([70]), underscoring the need to develop
770 mouse-appropriate solutions.

771 Our key innovation addresses these challenges through the use of three-part,
772 under-skin implants with replaceable reflective heads. Installed under brief isoflurane
773 anesthesia, these stainless steel implants anchor firmly as the skin heals. Mice resume
774 normal behavior within a day and show no signs of discomfort. Over weeks to months,
775 the implants remain stable without replacement. Although mice clean the implants
776 as part of their grooming routine, they do not remove them. Before experimental
777 recording, the stainless steel spheres capping the piercing shafts are substituted with
778 retroreflective markers using a simple screw-on mechanism. This process does not
779 require anesthesia and ensures consistently high-quality marker condition, resulting in
780 low-noise tracking. Although long-term changes in body dimensions and skin growth
781 may eventually necessitate reimplantation, we have not observed decline in quality
782 tracking over several weeks of regular use. This straightforward solution enables sta-
783 ble long-term tracking, making it suitable for extended studies of motor learning,
784 adaptation, or other long-term behavioral processes.

785 **5.2 Marker-based versus markerless methods and data quality**
786 **considerations**

787 The quality and resolution of kinematic data fundamentally determine the scope of
788 behavioral questions that can be addressed. The accuracy and precision of markerless
789 methods inherently depend on video resolution, training datasets, and the consistency
790 of human annotations used during model training. Although extremely high precision
791 with markerless tracking is theoretically achievable, practically replicating the subtle
792 kinematic findings presented here (e.g., differences in Motion Index during stationary
793 periods) would require exceptionally high-resolution video data.

794 The significant differences observed between CP and vehicle groups involved move-
795 ments during stationary periods averaging approximately 0.6 mm per 10 frames, and
796 this difference becomes unresolvable when simulating an increase in the recording's

797 "noise floor" to just 0.65 mm (Figure 4a). Reliably resolving such subtle displace-
798 ments demands spatial resolution at least half of this magnitude (around 0.3 mm
799 per pixel) with unambiguously identifiable anatomical landmarks. Given our record-
800 ing arena size (30 × 30 cm), capturing this resolution throughout the arena roughly
801 corresponds to standard high-definition (1080p) video resolution. However, practi-
802 cal considerations—including camera placement, lens distortion, animal movement
803 across the field, compression artifacts, and inefficient use of the camera's full field
804 of view—typically necessitate even higher resolution. Even conservatively recorded
805 1080p, 16-bit grayscale videos captured at 300 fps and compressed losslessly typi-
806 cally produce around 20–30 GB of data per minute. In contrast, MBMC datasets
807 remain orders of magnitude smaller—typically tens of MB per minute per marker,
808 even including full 3D reconstruction at 300 fps.

809 Processing large, high-resolution video files required for subtle-movement analysis
810 also poses practical challenges. Annotating frames for model training or performing
811 inference at full resolutions without downsampling quickly becomes computationally
812 cumbersome. Extending markerless tracking methods into full three-dimensional
813 reconstruction, such as with AniPose [24], further amplifies computational complex-
814 ity and processing demands, significantly increasing both computational burden and
815 data management challenges.

816 In this study, we instead demonstrate that MBMC yields highly accurate, low-noise
817 trajectories in compact form, immediately ready for analysis after straightforward
818 trajectory labeling. Only minimal data cleaning procedures were applied, such as
819 interpolation across short gaps and occasional single-frame jitter removal, ensuring
820 the captured behavioral features remain free from processing artifacts. Crucially, the
821 inherently low noise floor (quantified here as triangulation residuals) substantially
822 facilitates advanced analytical approaches such as dynamic embedding, which rely on

823 precise characterization of subtle and rapid corrective movements. Such detailed anal-
824 yses often become impossible or highly error-prone at noise levels that necessitate
825 temporal filtering [71].

826 Although establishing an MBMC system is somewhat more involved than record-
827 ing with a single camera for markerless tracking, the precision obtained significantly
828 outweighs this initial effort. The accuracy and noise sensitivity of this method
829 enable exploration of subtle behavioral features previously inaccessible with con-
830 ventional tracking. For example, small-amplitude oscillatory movements of shoulder
831 blade markers during passive immobility potentially reflect breathing, suggesting
832 possible applications in monitoring physiological states such as arousal. Similarly,
833 MBMC robustly resolves subtle, full-body tremors induced by harmaline adminis-
834 tration, revealing their spatial and temporal characteristics across the body (Figure
835 7). Such tremors, characterized by small amplitudes and high-frequency oscillations,
836 would likely be inaccurately quantified by conventional markerless approaches.

837 Ultimately, while MBMC is not proposed as a universal replacement for markerless
838 methods, it clearly excels in contexts requiring detailed, precise, and noise-sensitive
839 kinematic analyses of animals moving freely in 3D environments.

840 In the following, we briefly elaborate on key insights gained from the proof-of-
841 concept experiments presented in this manuscript.

842 **5.3 Context-dependent effects of low-dose CP55,940 on 843 locomotion**

844 A central insight from our experiments is that the behavioral impact of pharmacologi-
845 cal interventions depends on the locomotory context. Consistent with previous reports
846 [39, 40], administration of the cannabinoid receptor agonist ("CP") slightly reduced
847 overall locomotion in the OF arena (Figure 3). However, this suppression was not
848 observed when the same mice were tasked with a vertical CLB task on the wheel.

849 Unlike in OF, CP treatment reduced both the amplitude and speed of hindlimb
850 movements during CLB task (Figure 6c,d). However, this reduction did not alter the
851 ability of the mice to climb, a behavior in which they are naturally skilled, highlighting
852 the multifaceted nature of locomotion. In the more challenging and artificial locomo-
853 tory task (TRM), CP-treated mice were unable to maintain locomotion at speeds above
854 20 m/min, suggesting that the same drug-induced reduction in limb vigor had a more
855 pronounced impact under conditions demanding sustained high-speed locomotion.

856 In contrast, limb kinematics were unaffected in the OF, where locomotion was
857 slower and less demanding (Figure 6a,b) even though CP reduced non-locomotory
858 movements during stationary periods, as indicated by a lower average speed of all
859 markers (quantified as MI, Figure 4). These findings suggest that the apparent
860 “locomotory suppression” induced by low-dose CP arises from different mechanisms
861 depending on the behavioral context: in the OF, it can reflect motivational changes
862 that reduce levels of exploratory activity, while in CLB or TRM running, it is likely
863 the result of bradykinesia or reduced muscle tone that might only become functionally
864 significant in more demanding tasks.

865 **5.4 Not all swings are the same - insights from peak swing
866 speed timing**

867 Another novel insight emerged when comparing the variation in limb speeds in different
868 locomotory contexts. During running in the TRM task, the ankle speed consistently
869 peaked at the beginning and end of the swings, aligning with the presumed forceful
870 contact of the limb with the moving surface (Figure 5c). In contrast, during OF explo-
871 ration, ankle speed peaked during the early downswing phase, while it shifted to the
872 upward swing phase in the CLB task. These context-dependent differences in ankle
873 speed timing underscore a key advantage of MBMC: the ability to directly observe

874 and quantify the precise temporal structure of limb movements in animals exploring
875 a relatively broad volume.

876 Although 3D forelimb speed trajectories have previously been reported and exam-
877 ined in the context of circuit-level disruptions [1, 72, 73], the studies typically involved
878 constrained conditions. To our knowledge, we are the first to demonstrate distinct limb
879 timing profiles in the same animals during different, unconstrained locomotor behav-
880 iors. In particular, CP administration did not alter the timing of maximum ankle speed
881 during locomotion at self-driven speeds, possibly indicating that the observed reduc-
882 tions in swing vigor may result from effects targeting peripheral circuits or muscles
883 rather than timing mechanisms within central motor circuitry.

884 In sum, analyzing behavior across multiple, naturalistic locomotory contexts
885 demonstrates that a pharmacological manipulation can produce divergent outcomes
886 and that restricting analysis to a single behavior risks oversimplified conclusions.

887 5.5 Tracking tremor

888 Tremor, a rhythmic oscillation of body parts, is a defining symptom of many
889 neurological disorders, including Parkinson’s disease and essential tremor [56–58].
890 Characterizing the spatiotemporal structure of tremor can provide insight into the
891 underlying mechanisms driving these pathological oscillations.

892 In animal models, tremor is often quantified using force plates or single-point mea-
893 surements. While these approaches provide useful metrics, they collapse the complexity
894 of tremor into a single value, obscuring differences and interactions between body
895 parts. We hypothesized that full-body harmaline-induced tremor could be dominated
896 by activity in proximal or larger muscle groups, with oscillatory waves propagating
897 outward to more distal regions. In contrast to this expectation, we found strong in-
898 phase correlation across all tracked markers in all four animals (Figure 7g,h). This is

899 in line with harmaline tremor being mainly expressed through central, bilateral mech-
900 anism rather than localized, periferal mechanisms that would propagate the tremor
901 through the neuromotor apparatus [74, 75].

902 Changes in tremor amplitude with respect to behavioral modes can provide
903 valuable insights for characterizing tremor phenotypes. Essential tremor typically
904 intensifies during action (e.g. maintaining a posture or performing a movement),
905 whereas Parkinsonian tremor is more prominent at rest and often diminishes during
906 voluntary movement [76]. In our data, harmaline-induced tremor was most promi-
907 nent during stationary periods, particularly in the one mouse in which it was possible
908 to compare locomotion and immobility (Figure 7f). We found that the tremor sub-
909 sided during stepping movements, in conflict with the classical features of the essential
910 tremor, albeit possibly reflecting the effect of weight loading and therefore suggest-
911 ing the involvement of peripheral mechanisms [75, 77, 78]. Furthermore, we observed
912 bradykinesia-like slowness on the treadmill, possibly related to challenges in the precise
913 timing of limb movements (Figure 8c-e).

914 These findings highlight the bilateral nature of harmaline tremor, consistent with
915 essential tremor, but also reveal distinct behavioral context dependence and possible
916 bradykinesia. Rather than argue for or against the use of harmaline tremor as a model
917 of essential tremor [79], our results underscore the importance of evaluating tremor
918 models in different behavioral models and considering the coordination of tremors
919 throughout the body.

920 5.6 Concluding remarks

921 No single approach suits every behavioral study. MBMC, as presented here, excels
922 when the goal is to obtain precise, high-quality kinematics under diverse naturalistic
923 conditions. In contexts where detailed 3D kinematics are unnecessary, when through-
924 put takes priority over accuracy, or when external markers cannot be securely or

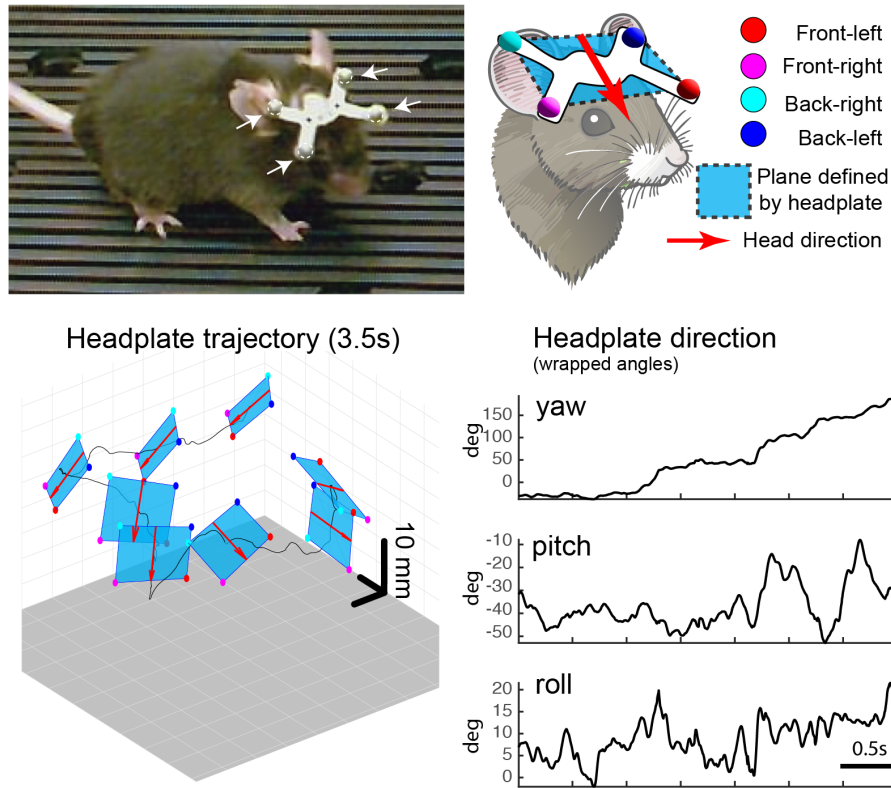
925 ethically implanted (e.g., on soft-bodied or wild animals), markerless methods remain
926 appropriate. Similarly, marker implantation may be superfluous if the experimental
927 design inherently restricts animal movements (e.g., head-fixing for two-photon imag-
928 ing) or focuses primarily on broad movement parameters such as animal location,
929 speed, or proximity to conspecifics.

930 When detailed and precise 3D kinematic information is required from freely mov-
931 ing animals, MBMC provides distinct advantages by minimizing the need for extensive
932 data post-processing, training, or parameter tuning. This approach yields compact,
933 ready-to-use trajectory data with minimal artifacts, facilitating advanced mathe-
934 matical analyses. Moreover, the compactness of MBMC data significantly reduces
935 the storage and management demands typically associated with large video files
936 acquired during markerless experiments, while also enabling real-time integration into
937 closed-loop experimental paradigms.

938 Although MBMC inherently requires physical placement of markers, their position-
939 ing is adaptable, allowing straightforward extension beyond the marker configurations
940 demonstrated here. In this study, we utilized markers placed on hind-body and
941 shoulder-blade regions, sufficient to address our specific research questions regard-
942 ing subtle differences in limb kinematics. However, markers can readily be implanted
943 on other body parts such as forelimbs (Movie 13, [6.5](#)), and precise head orientation
944 tracking can be realized by attaching markers to a lightweight headplate (Headplate
945 Model 10, Neurotar, Finland; Figure 9; combined weight less than 1.1 g)—instead
946 of relying on head-mounted inertial measurement units [\[80, 81\]](#). Importantly, MBMC
947 implementation is not restricted to high-end motion capture systems such as Qualisys,
948 Vicon (<https://www.vicon.com/>), or OptiTrack (<https://optitrack.com/>); flexible and
949 low-cost hardware alternatives are also available ([\[82\]](#)).

950 The utility of MBMC extends naturally to longitudinal tracking across the lifespan
951 of individual animals, providing unique opportunities for within-subject analyses over

Head tracking using markers attached to a headplate



Figure

9. Example of the potential of marker-based motion capture in tracking head movements. A conventional headplate (Model 10, Neurotar, Finland) is attached to the skull with dental cement. 2.5mm-diameter retroreflective facial markers (purchased from Qualisys, Sweden) are attached to the corners of the headplate (top left), thus allowing definition of the 2D plane of head direction (top right). Red arrow depicts "head direction" used in analysis. Bottom left: example trajectories from a 3.5s-long segment of open field exploratory behavior in which mouse turned around. Black line: continuous trajectory of the headplate center; blue rectangles and red arrows depict the head plane and direction, calculated at 0.5s intervals. Bottom right: head direction representation from the same period, shown in yaw, pitch and roll angles.

952 extended periods. Similarly, the approach can be readily adapted for multi-animal
 953 tracking and offers potential in studying disorders such as dystonia, epilepsy, or autistic
 954 phenotypes, where fine-grained motion analysis could uncover more subtle patterns
 955 than those detectable with existing methods [83–91].

Despite these clear advantages, MBMC involves certain practical considerations. Setting up multi-camera systems requires initial technical investment and expertise, and marker implantation—although minimally invasive and straightforward—necessitates brief anesthesia and appropriate surgical precautions. Additionally, successful MBMC recording outside conventional enclosures requires careful experimental planning with the animals' well-being in mind. Experimenters must remain mindful of animal comfort and maintain consistent procedures to ensure stable and low stress behavior. Although this initial effort may exceed that deemed sufficient in more conventional setups, it significantly reduces stress-induced behaviors, enhancing the validity and quality of the obtained kinematic data.

We hope that our practical implementation of MBMC in mice, supported by the detailed animal-training guidelines provided (Methods, 3.3), will motivate new analytical approaches to exploring detailed, full-body dynamics of mouse behavior in species-appropriate contexts.

5.7 Ethical approval declarations

The animal study protocol was conducted in accordance with procedures approved by the [Author institute]

References

- [1] Becker, M. I. & Person, A. L. Cerebellar control of reach kinematics for endpoint precision. *Neuron* **103**, 335–348 (2019).
- [2] De Schutter, E. Fallacies of mice experiments. *Neuroinformatics* **17**, 181–183 (2019).
- [3] Garner, J. P. The significance of meaning: why do over 90% of behavioral neuroscience results fail to translate to humans, and what can we do to fix it? *ILAR*

- 980 *journal* **55**, 438–456 (2014).
- 981 [4] Kennedy, A. The what, how, and why of naturalistic behavior. *Current opinion*
982 *in neurobiology* **74**, 102549 (2022).
- 983 [5] Marshall, J. D., Li, T., Wu, J. H. & Dunn, T. W. Leaving flatland: Advances in
984 3d behavioral measurement. *Current Opinion in Neurobiology* **73**, 102522 (2022).
- 985 [6] Ceseracciu, E., Sawacha, Z. & Cobelli, C. Comparison of markerless and marker-
986 based motion capture technologies through simultaneous data collection during
987 gait: proof of concept. *PloS one* **9**, e87640 (2014).
- 988 [7] Moro, M., Marchesi, G., Hesse, F., Odone, F. & Casadio, M. Markerless vs.
989 marker-based gait analysis: A proof of concept study. *Sensors* **22**, 2011 (2022).
- 990 [8] Nakano, N. *et al.* Evaluation of 3d markerless motion capture accuracy using
991 openpose with multiple video cameras. *frontiers in sports and active living*. 2020;
992 2: 50 (2020).
- 993 [9] Schmitz, A. *et al.* The measurement of in vivo joint angles during a squat using a
994 single camera markerless motion capture system as compared to a marker based
995 system. *Gait & posture* **41**, 694–698 (2015).
- 996 [10] Tang, H., Munkasy, B. & Li, L. Differences between lower extremity joint running
997 kinetics captured by marker-based and markerless systems were speed dependent.
998 *Journal of Sport and Health Science* **13**, 569–578 (2024).
- 999 [11] Becker, M. I., Calame, D. J., Wrobel, J. & Person, A. L. Online control of reach
1000 accuracy in mice. *Journal of Neurophysiology* **124**, 1637–1655 (2020).
- 1001 [12] Steinebach, T., Grosse, E. H., Glock, C. H., Wakula, J. & Lunin, A. Accu-
1002 racy evaluation of two markerless motion capture systems for measurement of

- 1003 upper extremities: Kinect v2 and captiv. *Human Factors and Ergonomics in*
1004 *Manufacturing & Service Industries* **30**, 291–302 (2020).
- 1005 [13] Topley, M. & Richards, J. G. A comparison of currently available optoelectronic
1006 motion capture systems. *Journal of biomechanics* **106**, 109820 (2020).
- 1007 [14] von Ziegler, L., Sturman, O. & Bohacek, J. Big behavior: challenges and oppor-
1008 tunities in a new era of deep behavior profiling. *Neuropsychopharmacology* **46**,
1009 33–44 (2021).
- 1010 [15] Pereira, T. D., Shaevitz, J. W. & Murthy, M. Quantifying behavior to understand
1011 the brain. *Nature neuroscience* **23**, 1537–1549 (2020).
- 1012 [16] Mathis, A. *et al.* Deeplabcut: markerless pose estimation of user-defined body
1013 parts with deep learning. *Nature neuroscience* **21**, 1281–1289 (2018).
- 1014 [17] Nath, T. *et al.* Using deeplabcut for 3d markerless pose estimation across species
1015 and behaviors. *Nature protocols* **14**, 2152–2176 (2019).
- 1016 [18] Lauer, J. *et al.* Multi-animal pose estimation, identification and tracking with
1017 deeplabcut. *Nature Methods* **19**, 496–504 (2022).
- 1018 [19] Pereira, T. D. *et al.* Sleap: A deep learning system for multi-animal pose tracking.
1019 *Nature methods* **19**, 486–495 (2022).
- 1020 [20] Dunn, T. W. *et al.* Geometric deep learning enables 3d kinematic profiling across
1021 species and environments. *Nature methods* **18**, 564–573 (2021).
- 1022 [21] Wiltschko, A. B. *et al.* Revealing the structure of pharmacobehavioral space
1023 through motion sequencing. *Nature neuroscience* **23**, 1433–1443 (2020).

- 1024 [22] Weinreb, C. *et al.* Keypoint-moseq: parsing behavior by linking point tracking to
1025 pose dynamics. *Nature Methods* **21**, 1329–1339 (2024).
- 1026 [23] Biderman, D. *et al.* Lightning pose: improved animal pose estimation via semi-
1027 supervised learning, bayesian ensembling and cloud-native open-source tools.
1028 *Nature Methods* **21**, 1316–1328 (2024).
- 1029 [24] Karashchuk, P. *et al.* Anipose: A toolkit for robust markerless 3d pose estimation.
1030 *Cell reports* **36** (2021).
- 1031 [25] Ito, N. *et al.* Markerless motion capture: What clinician-scientists need to know
1032 right now. *JSAMS plus* **1**, 100001 (2022).
- 1033 [26] Li, T., Severson, K. S., Wang, F. & Dunn, T. W. Improved 3d markerless
1034 mouse pose estimation using temporal semi-supervision. *International journal of*
1035 *computer vision* **131**, 1389–1405 (2023).
- 1036 [27] Buckley, C. *et al.* The role of movement analysis in diagnosing and monitoring
1037 neurodegenerative conditions: Insights from gait and postural control. *Brain*
1038 *sciences* **9**, 34 (2019).
- 1039 [28] Drazan, J. F., Phillips, W. T., Seethapathi, N., Hullfish, T. J. & Baxter, J. R.
1040 Moving outside the lab: Markerless motion capture accurately quantifies sagittal
1041 plane kinematics during the vertical jump. *Journal of Biomechanics* **125**, 110547
1042 (2021).
- 1043 [29] Kanko, R. M., Laende, E. K., Davis, E. M., Selbie, W. S. & Deluzio, K. J. Con-
1044 current assessment of gait kinematics using marker-based and markerless motion
1045 capture. *Journal of biomechanics* **127**, 110665 (2021).

- 1046 [30] Philipp, N. M., Cabarkapa, D., Cabarkapa, D. V., Eserhaut, D. A. & Fry, A. C.
1047 Inter-device reliability of a three-dimensional markerless motion capture system
1048 quantifying elementary movement patterns in humans. *Journal of Functional*
1049 *Morphology and Kinesiology* **8**, 69 (2023).
- 1050 [31] Song, K., Hullfish, T. J., Silva, R. S., Silbernagel, K. G. & Baxter, J. R. Marker-
1051 less motion capture estimates of lower extremity kinematics and kinetics are
1052 comparable to marker-based across 8 movements. *Journal of Biomechanics* **157**,
1053 111751 (2023).
- 1054 [32] Wade, L., Needham, L., McGuigan, P. & Bilzon, J. Applications and limitations of
1055 current markerless motion capture methods for clinical gait biomechanics. *PeerJ*
1056 **10**, e12995 (2022).
- 1057 [33] Bae, K. *et al.* Concurrent validity and test reliability of the deep learning mark-
1058 erless motion capture system during the overhead squat. *Scientific Reports* **14**,
1059 29462 (2024).
- 1060 [34] Moore, D. D., Walker, J. D., MacLean, J. N. & Hatsopoulos, N. G. Validating
1061 markerless pose estimation with 3d x-ray radiography. *Journal of Experimental*
1062 *Biology* **225**, jeb243998 (2022).
- 1063 [35] Dagenais, P., Hensman, S., Haechler, V. & Milinkovitch, M. C. Elephants evolved
1064 strategies reducing the biomechanical complexity of their trunk. *Current Biology*
1065 **31**, 4727–4737 (2021).
- 1066 [36] O'Neill, M. C. *et al.* Adaptations for bipedal walking: Musculoskeletal structure
1067 and three-dimensional joint mechanics of humans and bipedal chimpanzees (pan-
1068 troglodytes). *Journal of Human Evolution* **168**, 103195 (2022).

- 1069 [37] Roepstorff, C. *et al.* Reliable and clinically applicable gait event classification
1070 using upper body motion in walking and trotting horses. *Journal of biomechanics*
1071 **114**, 110146 (2021).
- 1072 [38] Marshall, J. D. *et al.* Continuous whole-body 3d kinematic recordings across the
1073 rodent behavioral repertoire. *Neuron* **109**, 420–437 (2021).
- 1074 [39] Patel, S. & Hillard, C. J. Cannabinoid CB₁ receptor agonists produce cerebellar
1075 dysfunction in mice. *Journal of Pharmacology and Experimental Therapeutics*
1076 (2001).
- 1077 [40] Ignatowska-Jankowska, B. M. *et al.* A cannabinoid cb1 receptor-positive allosteric
1078 modulator reduces neuropathic pain in the mouse with no psychoactive effects.
1079 *Neuropsychopharmacology* **40**, 2948–2959 (2015).
- 1080 [41] Ignatowska-Jankowska, B. *et al.* Selective monoacylglycerol lipase inhibitors:
1081 antinociceptive versus cannabimimetic effects in mice. *Journal of Pharmacology
and Experimental Therapeutics* **353**, 424–432 (2015).
- 1083 [42] Martin, F. C., Thu Le, A. & Handforth, A. Harmaline-induced tremor as a poten-
1084 tial preclinical screening method for essential tremor medications. *Movement
Disorders* **20**, 298–305 (2005).
- 1086 [43] Du Sert, N. P. *et al.* Reporting animal research: Explanation and elaboration for
1087 the arrive guidelines 2.0. *PLoS biology* **18**, e3000411 (2020).
- 1088 [44] Josefsson, T., Nordh, E. & Eriksson, P.-O. A flexible high-precision video system
1089 for digital recording of motor acts through lightweight reflex markers. *Computer
methods and programs in biomedicine* **49**, 119–129 (1996).

- 1091 [45] Hartley, R. *Multiple view geometry in computer vision* Vol. 665 (Cambridge
1092 university press, 2003).
- 1093 [46] Qualisys. Understanding the calibration. URL https://docs.qualisys.com/getting-started/content/getting_started/running_your_qualisys_system/calibrating_your_system/understanding_the_calibration.htm. Accessed on 10
1094 December 2024.
- 1095 [47] de Groot, A. *et al.* Ninscope, a versatile miniscope for multi-region circuit
1096 investigations. *Elife* **9**, e49987 (2020).
- 1097 [48] Lopes, G. *et al.* Bonsai: an event-based framework for processing and controlling
1098 data streams. *Frontiers in neuroinformatics* **9**, 7 (2015).
- 1099 [49] Kalueff, A. V. *et al.* Neurobiology of rodent self-grooming and its value for
1100 translational neuroscience. *Nature Reviews Neuroscience* **17**, 45–59 (2016).
- 1101 [50] Ueno, M. & Yamashita, T. Kinematic analyses reveal impaired locomotion fol-
1102 lowing injury of the motor cortex in mice. *Experimental neurology* **230**, 280–290
1103 (2011).
- 1104 [51] Lemieux, M., Josset, N., Roussel, M., Couraud, S. & Bretzner, F. Speed-
1105 dependent modulation of the locomotor behavior in adult mice reveals attractor
1106 and transitional gaits. *Frontiers in neuroscience* **10**, 42 (2016).
- 1107 [52] Braine, A. & Georges, F. Emotion in action: when emotions meet motor circuits.
1108 *Neuroscience & Biobehavioral Reviews* 105475 (2023).
- 1109 [53] Helmich, R. C., Toni, I., Deuschl, G. & Bloem, B. R. The pathophysiology of
1110 essential tremor and parkinson's tremor. *Current neurology and neuroscience*
1111 *reports* **13**, 1–10 (2013).

- 1114 [54] Duque, J. D. L., Egea, A. J. S., Reeb, T., Rojas, H. A. G. & Gonzalez-Vargas,
1115 A. M. Angular velocity analysis boosted by machine learning for helping in the
1116 differential diagnosis of parkinson's disease and essential tremor. *IEEE access* **8**,
1117 88866–88875 (2020).
- 1118 [55] Fujikawa, J. *et al.* Diagnosis and treatment of tremor in parkinson's disease using
1119 mechanical devices. *Life* **13**, 78 (2022).
- 1120 [56] Rahimi, F. *et al.* Dynamic decomposition of motion in essential and parkinsonian
1121 tremor. *Canadian Journal of Neurological Sciences* **42**, 116–124 (2015).
- 1122 [57] Angelini, L. *et al.* Clinical and kinematic characterization of parkinsonian soft
1123 signs in essential tremor. *Journal of Neural Transmission* 1–12 (2024).
- 1124 [58] Welton, T. *et al.* Essential tremor. *Nature reviews Disease primers* **7**, 83 (2021).
- 1125 [59] Wang, G. Quantitative behavioral models for high-resolution measurement and
1126 characterization of tremor in rodents. *Brain Research Bulletin* **186**, 8–15 (2022).
- 1127 [60] Handforth, A. Harmaline tremor: underlying mechanisms in a potential animal
1128 model of essential tremor. *Tremor and other hyperkinetic movements* **2** (2012).
- 1129 [61] Milner, T. E., Cadoret, G., Lessard, L. & Smith, A. M. Emg analysis of harmaline-
1130 induced tremor in normal and three strains of mutant mice with purkinje cell
1131 degeneration and the role of the inferior olive. *Journal of neurophysiology* **73**,
1132 2568–2577 (1995).
- 1133 [62] Paterson, N. E., Malekiani, S. A., Foreman, M. M., Olivier, B. & Hanania, T.
1134 Pharmacological characterization of harmaline-induced tremor activity in mice.
1135 *European journal of pharmacology* **616**, 73–80 (2009).

- 1136 [63] Woodward, K., Apps, R., Goodfellow, M. & Cerminara, N. L. Cerebello-thalamo-
1137 cortical network dynamics in the harmaline rodent model of essential tremor.
1138 *Frontiers in Systems Neuroscience* **16**, 899446 (2022).
- 1139 [64] Bologna, M. *et al.* Is there evidence of bradykinesia in essential tremor? *European*
1140 *journal of neurology* **27**, 1501–1509 (2020).
- 1141 [65] Bologna, M., Paparella, G., Fasano, A., Hallett, M. & Berardelli, A. Evolving
1142 concepts on bradykinesia. *Brain* **143**, 727–750 (2020).
- 1143 [66] Hartley, R. I. & Sturm, P. Triangulation. *Computer vision and image*
1144 *understanding* **68**, 146–157 (1997).
- 1145 [67] Kanatani, K., Sugaya, Y. & Niitsuma, H. Triangulation from two views revisited:
1146 Hartley-sturm vs. optimal correction. *practice* **4**, 99 (2008).
- 1147 [68] Monsees, A. *et al.* Estimation of skeletal kinematics in freely moving rodents.
1148 *Nature methods* **19**, 1500–1509 (2022).
- 1149 [69] Mimica, B., Dunn, B. A., Tombaz, T., Bojja, V. S. & Whitlock, J. R. Efficient
1150 cortical coding of 3d posture in freely behaving rats. *Science* **362**, 584–589 (2018).
- 1151 [70] Ellenbroek, B. & Youn, J. Rodent models in neuroscience research: is it a rat
1152 race? *Disease models & mechanisms* **9**, 1079–1087 (2016).
- 1153 [71] Kristianslund, E., Krosshaug, T. & Van den Bogert, A. J. Effect of low pass filter-
1154 ing on joint moments from inverse dynamics: implications for injury prevention.
1155 *Journal of biomechanics* **45**, 666–671 (2012).
- 1156 [72] Machado, A. S., Marques, H. G., Duarte, D. F., Darmohray, D. M. & Carey,
1157 M. R. Shared and specific signatures of locomotor ataxia in mutant mice. *Elife*
1158 **9**, e55356 (2020).

- 1159 [73] Calame, D. J., Becker, M. I. & Person, A. L. Cerebellar associative learning
1160 underlies skilled reach adaptation. *Nature Neuroscience* **26**, 1068–1079 (2023).
- 1161 [74] Pan, M.-K. & Kuo, S.-H. Tracking the central and peripheral origin of
1162 tremor. *Clinical neurophysiology: official journal of the International Federation
1163 of Clinical Neurophysiology* **129**, 1451 (2018).
- 1164 [75] Hopfner, F. & Helmich, R. C. The etiology of essential tremor: Genes versus
1165 environment. *Parkinsonism & related disorders* **46**, S92–S96 (2018).
- 1166 [76] Deuschl, G., Bain, P., Brin, M. & Committee, A. H. S. Consensus statement of
1167 the movement disorder society on tremor. *Movement disorders* **13**, 2–23 (1998).
- 1168 [77] Hallett, M. Overview of human tremor physiology. *Movement disorders* **13**, 43–48
1169 (1998).
- 1170 [78] Van der Stouwe, A. *et al.* How typical are ‘typical’tremor characteristics? sensitivity
1171 and specificity of five tremor phenomena. *Parkinsonism & related disorders*
1172 **30**, 23–28 (2016).
- 1173 [79] Louis, E. D. Understanding essential tremor: progress on the biological front.
1174 *Current neurology and neuroscience reports* **14**, 1–8 (2014).
- 1175 [80] Wilson, J. J., Alexandre, N., Trentin, C. & Tripodi, M. Three-dimensional rep-
1176 resentation of motor space in the mouse superior colliculus. *Current Biology* **28**,
1177 1744–1755 (2018).
- 1178 [81] González-Rueda, A. *et al.* Kinetic features dictate sensorimotor alignment in the
1179 superior colliculus. *Nature* **631**, 378–385 (2024).
- 1180 [82] Chatzitofis, A., Zarpalas, D., Daras, P. & Kollias, S. Democap: Low-cost marker-
1181 based motion capture. *International Journal of Computer Vision* **129**, 3338–3366

1182 (2021).

1183 [83] Snell, H. D. *et al.* Mechanism of stress-induced attacks in an episodic neurologic
1184 disorder. *Science Advances* **8**, eabh2675 (2022).

1185 [84] Gray, M. M., Naik, A., Ebner, T. J. & Carter, R. E. Altered brain state during
1186 episodic dystonia in tottering mice decouples primary motor cortex from limb
1187 kinematics. *Dystonia* **2**, 10974 (2023).

1188 [85] van der Heijden, M. E., Brown, A. M., Kizek, D. J. & Sillitoe, R. V. Cerebel-
1189 lar nuclei cells produce distinct pathogenic spike signatures in mouse models of
1190 ataxia, dystonia, and tremor. *Elife* **12**, RP91483 (2024).

1191 [86] Washburn, S. *et al.* The cerebellum directly modulates the substantia nigra
1192 dopaminergic activity. *Nature Neuroscience* **27**, 497–513 (2024).

1193 [87] Velíšková, J. & Velíšek, L. in *Models of seizures and epilepsy* (eds Pitkänen, A.,
1194 Buckmaster, P. S., Galanopoulou, A. S. & Moshé, S. L.) *Behavioral characteri-
1195 zation and scoring of seizures in rodents* 111–123 (Elsevier, 2017).

1196 [88] Streng, M. L., Tetzlaff, M. R. & Krook-Magnuson, E. Distinct fastigial output
1197 channels and their impact on temporal lobe seizures. *Journal of Neuroscience*
1198 **41**, 10091–10107 (2021).

1199 [89] Gschwind, T. *et al.* Hidden behavioral fingerprints in epilepsy. *Neuron* **111**,
1200 1440–1452 (2023).

1201 [90] Cook, J. From movement kinematics to social cognition: the case of autism. *Philoso-
1202 sophical Transactions of the Royal Society B: Biological Sciences* **371**, 20150372
1203 (2016).

₁₂₀₄ [91] Klibaite, U. *et al.* Deep phenotyping reveals movement phenotypes in mouse
₁₂₀₅ neurodevelopmental models. *Molecular Autism* **13**, 12 (2022).

₁₂₀₆ **6 Movie captions**

₁₂₀₇ **6.1 Movie 1**

₁₂₀₈ Raw 3D reconstruction of marker positions during open field exploration shown in real
₁₂₀₉ time. Red color of a marker indicates break in automatic tracking.

₁₂₁₀ **6.2 Movie 2**

₁₂₁₁ Video and motion capture reconstructions of full 1-min trials involving open field
₁₂₁₂ exploration in the same mouse treated with vehicle and CP55,940.

₁₂₁₃ **6.3 Movie 3**

₁₂₁₄ Video and motion capture reconstructions of full 1-min trials involving voluntary wheel
₁₂₁₅ climbing in the same mouse treated with vehicle and CP55,940.

₁₂₁₆ **6.4 Movie 4**

₁₂₁₇ Video and motion capture reconstructions of full 30-s trials involving running on
₁₂₁₈ a motorized treadmill, in the same mouse treated with vehicle and CP55,940. Two
₁₂₁₉ highest speeds this mouse reached are shown for both conditions.

₁₂₂₀ **6.5 Movie 5**

₁₂₂₁ Close-up video and motion capture reconstruction for two segments of high-speed
₁₂₂₂ running on a treadmill.

₁₂₂₃ **6.6 Movie 6**

₁₂₂₄ Video and motion capture reconstructions of a full 30-s trial of a single mouse running
₁₂₂₅ on treadmill at various speeds.

₁₂₂₆ **6.7 Movie 7**

₁₂₂₇ Close-up motion capture reconstruction of a segment of high-speed running (40 m/min
₁₂₂₈ treadmill speed), in normal speed and slowed-down to 20 %.

₁₂₂₉ **6.8 Movie 8**

₁₂₃₀ Close-up motion capture reconstruction of raw, unprocessed marker positions during a
₁₂₃₁ full 1-min recording of a mouse under harmaline influence. Text in upper right corner
₁₂₃₂ indicates gaps in marker tracking.

₁₂₃₃ **6.9 Movie 9**

₁₂₃₄ Close-up motion capture reconstruction of raw, unprocessed marker positions in a
₁₂₃₅ mouse under harmaline influence, shown slowed down to 20 %. Text in upper right
₁₂₃₆ corner indicates gaps in marker tracking.

₁₂₃₇ **6.10 Movie 10**

₁₂₃₈ Video and motion capture reconstructions of full 1-min trials involving open field
₁₂₃₉ exploration in the same mouse treated with vehicle and harmaline.

₁₂₄₀ **6.11 Movie 11**

₁₂₄₁ Video and motion capture reconstructions of full 1-min trials involving wheel climbing
₁₂₄₂ in the same mouse treated with vehicle and harmaline.

₁₂₄₃ **6.12 Movie 12**

₁₂₄₄ Video and motion capture reconstructions of a full 30-s trial of a single mouse
₁₂₄₅ locomoting on treadmill at various speeds under harmaline influence.

₁₂₄₆ **6.13 Movie 13**

₁₂₄₇ Video and motion capture reconstructions of mice locomoting with forelimb or
₁₂₄₈ headplate trackers.